ACTA MATERIALIA TRANSYLVANICA

Material Sciences Publications

Volume 1, Issue 1

ERDÉLYI MÚZEUM-EGYESÜLET
Kolozsvár
2018

A folyóirat megjelenését támogatta a Magyar Tudományos Akadémia, a Bethlen Gábor Alapkezelő Zrt. és az EME Műszaki Tudományok Szakosztálya / The publication of this magazine was supported by the Hungarian Academy of Sciences, by the Bethlen Gábor Fund and by the TMS – Department of Engineering Sciences

Főszerkesztő / Editor-in-Chief: Bitay Enikő

Nemzetközi Tanácsadó testület / International Editorial Advisory Board:
Prof. Biró László Péter, MTA Energiatudományi Kutatóközpont, Budapest, Magyarország
Prof. emer. B. Nagy János, University of Namur, Namur, Belgium
Prof. Czigány Tibor, Budapesti Műszaki és Gazdaságtudományi Egyetem, Budapest, Magyarország
Prof. Diószegi Attila, Jönköping University, Jönköping, Svédország
Dobránszky János, MTA–BME Kompozittechnológiai Kutatócsoport, Budapest, Magyarország
Prof. Dusza János, Institute of Materials Research of Slovak Academy of Sciences, Kassa, Szlovákia
Prof. Gyenge Csaba, Technical University of Cluj-Napoca, Kolozsvár, Románia
Prof. emer. Gyulai József, Budapesti Műszaki és Gazdaságtudományi Egyetem, Budapest, Magyarország
Prof. Kaptay György, Miskolci Egyetem, Miskolc, Magyarország
Dr. Kolozsváry Zoltán, Plasmaterm Rt., Marosvásárhely, Románia
Prof. Mertinger Valéria, Miskolci Egyetem, Miskolc, Magyarország
Prof. Porkoláb Miklós, Massachusetts Institute of Technology, Cambridge, MA, USA
Prof. Réger Mihály, Óbudai Egyetem, Budapest, Magyarország
Prof. emer. Réti Tamás, Óbudai Egyetem, Budapest, Magyarország
Prof. emer. Roósz András, Miskolci Egyetem, Miskolc, Magyarország
Dr. Spenik Sándor, Ungvári Nemzeti Egyetem, Ungvár, Ukrajna
Prof. Zsoldos Ibolya, Széchenyi István Egyetem, Győr, Magyarország

Lapszámszerkesztők / Editorial Board:
Gergely Attila, Sapientia Erdélyi Magyar Tudományegyetem, Marosvásárhely, Románia
Forizs Edit, Babeș–Bolyai Tudományegyetem, Kolozsvár, Románia
Kovács Tünde, Óbudai Egyetem, Budapest, Magyarország
Orbulov Imre, Budapesti Műszaki és Gazdaságtudományi Egyetem, Budapest, Magyarország

Kiadó / Publisher: Erdélyi Múzeum-Egyesület
Felelős kiadó / Responsible publisher: Biró Annamária
Olvasószerkesztő / Proofreader: Szenkovics Enikő (magyar), David Speight (English)
Szerkesztőségi titkár / Editorial secretary: Kisfaludi-Bak Zsombor
Műszaki szerkesztő / DTP: Szilágyi Júlia
Borítóterv / Cover: Könczey Elemér
Nyomdai munkálatok / Printed at: F&F International kft., Gyergyószentmiklós
Copyright © a szerzők / the authors, EME/ TMS 2018
ISSN 2601-1883, ISSN-L 2601-1883
DOI: 10.33924/amt-2018-01
Online elérhető / online available at: https://eda.eme.ro/handle/10598/30356
A folyóirat honlapja / The journal webpage: http://www.eme.ro/publication/acta-mat/mat-main.htm

Az *Acta Materialia Transylvanica. Anyagtudományi Közlemények* az Erdélyi Múzeum-Egyesület (EME) Műszaki Tudományok Szakosztályának folyóirata, amely az anyagtudományok területéről közöl tudományos közleményeket: szakcikkeket, összefoglalókat (szemléket), tanulmányokat. A folyóirat célja összképet adni kiemelten a Kárpát-medencei kutatási irányokról, tudományos eredményeiről, s ezt széles körben terjeszteni is. A folyóirat az EME felvállalt céljaihoz híven a magyar szaknyelv ápolását is támogatja, így a nyomtatott folyóirat magyar nyelven jelenik meg, mely az Erdélyi digitális adattárban elérhető (https://eda.eme.ro/handle/10598/30356). A széles körű nemzetközi terjesztés érdekében a folyóirat teljes angol nyelvű változatát is közzétesszük.

Acta Materiala Transylvanica – Material Sciences Publications – is a journal of the Technical Sciences Department of the Transylvanian Museum Society, publishing scientific papers, issues, reviews and studies in the field of material sciences. Its mission is to provide and disseminate a comprehensive picture focusing on research trends and scientific results in the Carpathian basin. In accordance with the general mission of the Transylvanian Museum Society it aims to support specialized literature in Hungarian. The printed version of the journal is published in Hungarian and is available in the Transylvanian Digital Database (https://eda.eme.ro/handle/10598/30356). However, we would like to spread it internationally, therefore the full content of the journal will also be available in English.

Tartalom / Content

Acta Materialia Transylvanica 1/1. (2018) 5–11.
https://doi.org/10.2478/amt-2018-0002
Hungarian: ~~https://doi.org/10.2478/amt-2018-0001~~
https://doi.org/10.33923/amt-2018-0001
Corrected: 29.08.2023.

Materials Science and Engineering – Some Aspects in Central and Eastern European (CEE) Countries

József GYULAI

Hungarian Academy of Sciences, Resource Centre for Energy Research, Institute of Technical Physics and Materials Science, MFA, Budapest, Hungary, gyulai.jozsef@energia.mta.hu

Abstract

This introductory paper summarizes the characteristics of how "Science" and "Engineering" differ from each other, forming the interdisciplinary topic of Materials Science and Engineering (MS&E). It will be shown how microelectronics has developed from modern materials science, causing a change in paradigm, and how microelectronics has become the "mother" science of informatics, changing life on Earth. To prove the importance of materials, a table is shown summarizing how modern MS&E forms the basis of practically all industries. The situation and development state of MS&E in CEE countries - despite different levels of industrialization – have some characteristics in common, and the way to development might also have techniques in common.

We will also mention the knowledge base that CEE countries possessed during the period of political change, and the likely future that an elderly scientist foresees for the region with the help of young ambitious scientists.

Keywords*: material science, engineering, microelectronics, interdisciplinary material science.*

Introduction

This paper is devoted to young engineering students with the aim of strengthening their devotion to a future career. Before we turn to the topic of this paper, a short chapter is included to draw attention to how the 21st century places a heavy onus on the shoulders of these future engineers. The global success of engineering is a key factor in keeping our planet habitable. A safe solution seems to be the so-called "Circular economy", which states that all production and consumption processes are part of a closed cycle of material flow requiring minimum energy. It is believed that there is no more important a task in science today than tstudy if, and if so how ten billion people can live on Earth without catastrophically destroying the interdependent network of living creatures. This is the message that must be clarified to young engineers.

To find the answer, a few words are devoted to the often confused relationship of "science" to "engineering"? Scientists, especially experimentalists, seek and find new phenomena and try to find explanations for experimentally observed facts. In this often "curiosity driven" process, models are defined based on mathematics, information technology, etc. the level of which, of course, is dependent on the available knowledge at the time. The applications of their work in the future are not immediately foreseen. Thus, when planning an experiment, numerous influencing factors must be neglected in order to arrive at a solution that best fits the state of theoretical development at that time. Once basic laws and facts are accepted, future talented "engineer-scientists" look at and treat basic laws of physics, chemistry etc. as "tools" which can be used to form materials into structures - products with expected, or rather with predetermined properties. Therefore, the engineer-scientist has to account for as many as possible at his time of these by constraint parameters in order to arrive at a better defined solution, a solution which enables the building of reliable future products. If this definition of engineering science is accepted, then a second step

follows in which a collective of engineers will define and optimize parameters such as temperature, time duration, pressure, chemical doping, etc., under which these law-based "tools" should act and change properties of the material in question. These conditions, rules and prescriptions will convert 'experiment' into a 'product', whose final acceptance will be evident in the economy.

Materials science and engineering (MS&E), in general

Modern MS@E is the daughter of informatics. It does not imply that the earlier forms of this science were not useful – think e.g. of swords of Damascus, or the dawn of metallurgy described in the book of Agricola, the *Dē rē metallica* (1556) [1]. But, quantification of metallurgical processes by the use of informatics, in a very broad sense, has caused a fundamental paradigm change. Today, the understanding of processes, often on an atomic scale, allows mankind to improve technology and to produce products on an industrial scale.

It may not be an exaggeration that microelectronics technology was and still is the leading field of science that drives automation, robotics, system control and quality management forward, by demanding new and better solutions. A summary of a few examples follow relating to materials science and the demands of transistor technology.

In this example, the goal is - as the drawing from **Figure 1** shows - to control the flight of charge carriers within a so-called space charge layer, from the source (S) region to the drain (D), (in the rear of **Figure 1** under a SiO_2-insulated metal layer on top, called the gate (G)). Carrier A flies freely: "ballistically accelerated", carrier B's track interacts with potential wells of deliberately embedded ions to control operation voltage. This interaction, however, "heats" the crystal, and this heat must be conducted away – a serious problem if, for example. millions of transistors are connected to form, e.g., a logic circuit.

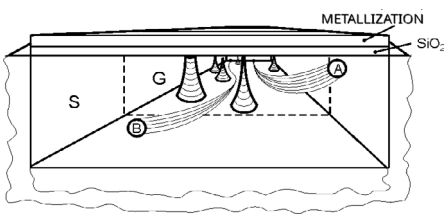

Figure 1. Visualized tracks (ballistic, A, and scattered, B) of charge carriers from Source (S) to Drain (D) in the so-called space charge layer of a Metal-Oxide-Semiconductor, MOS, transistor

"Exponential" means that the number of elements doubles yearly. Moore was modest enough to think that this unprecedented development would stay with us, say, till end of the seventies. It turned out that his modesty was an understatement: we are still seeing the law being fulfilled even today, though with some additional corrections, e.g., the exact 2D-version of an integrated circuit (IC) would not allow further miniaturization, structures must leap out into a 3rd dimension. Nature, however, has assisted mankind by means of the so-called "Dennard scaledown": if all dimensions of a transistor are multiplied by a number smaller than one, it is only the heat emission that will change and the electrical properties will remain the same. Today, industry is at "12 nm technology", i.e. the smallest features are around 12 nm.

With this in mind, an overview can be given of what the effect of this miniaturization is upon precision of production technology, when individual transistors are smaller than a virus.

1. Defect free crystals. It is the element silicon which holds the size-record for growing a defect free single crystal, using the Czochralski-growing technology. A few hundred kN crystal is sliced into 300 mm diameter crystallographically oriented wafers of about 700 micron thickness, ground and polished to a few tenths of a nm root-mean-square (r.m.s.) roughness, more aptly called "smoothness". Finally, it is cleaned beyond 'chemical' cleanliness, packaged and delivered to the semiconductor foundry. The maximum number of surface dislocations is below 1/10 cm^2.
2. Dielectric (SiO_2, or high-dielectric constant) layer growth. Scaling down requires thinner and thinner insulation between the metal gate and space charge layer in the silicon. Currently down to a few nm, i.e., to a thickness of few elementary cells. This thickness can grow in reduced O_2-pressure in seconds, homogeneously over the 300 mm wafer. Steps, even single atomic steps at the Si SiO_2 interface, are not allowed more than at every 10,000th atom (as atomic steps involve inherently dangling chemical bonds, which can act as traps for the carriers).
3. Photolithography. To form structures with some 10 nm size requires around 100 nm wavelength illumination in lithography. To arrive at fault-

less structures of a tenth of this wavelength, all diffraction must be avoided, and this requires extremely high quality optics.
4. All of the above need to be adhered to in order to perform at nearly 100% output…

It is believed that these requirements convince the Reader of the uniqueness of this industry. To add more, as sizes shrink into the nanometer range, the latest version of microelectronics is called “nanoelectronics”, where other binary quantities, like spins, act as the carrier of digital information (“spintronics”). Then, we arrive at the next stage, quantum computing, which may reach industrial level in the coming decades. However, a decade or longer time lag is usual between successful lab experiments and mass production.

No wonder that until turn of the millennium, microelectronics merged into and fertilized all branches of industry, both physics and chemistry based ones, and we witness its slow penetration into the bioindustry. Usually the software basis of regulation first leads penetration, is followed by automatization and, finally, robotization of the hardware. Later in this paper, a summary of this fertilizing penetration of MS&E will be given.

Forms of MS&E

Two forms of MS&E are often distinguished. One is the so-called “top down” process, the other is the “bottom up” process. The first form is the ancient idea, as it represents, e.g., the stone age technique of how sharp obsidian tools, flints were made. Analogous techniques prevail, say, in the lathe turning of metals. Here, trillions of bonds go broken resulting in heating, representing energy loss. This can be somewhat diminished using form casting. Better forms are the bottom up techniques, the pinnacle of which is plant life [3]. An early lecture of R. Feynman is often quoted as a prophesy of nanoscience or nanotechnology [4]. Today ground-breaking nanotechnology processes use predominantly bottom-up-type processing, like nanoelectronics.

Materials engineering and branches of industry

MS&E is a horizontal science: practically no product of human activity is imaginable that doesn’t involve some kind of material. It is normal that all products have a demand on a specific raw or starting material. The **Table 1** summarizes today’s leading research in different materials and their importance in different industries. The reader may find missing data, comments, but the complexity of this tutorial table must surely be convincing.

Conclusions for CEE young students, engineers

The structure of industry in CEE countries at the onset of political changes was unique. Being earlier members of an alliance, their industries were specifically developed in the interests of the military needs of the cold war, although with some consideration of local specialities. The main direction was in heavy industry (steel, oil, etc.,), thus, materials science was more like the Russian-Soviet “Materialovedenie”, or the GDR ”Werkstoff-Forschung” resembling more the historically important and valuable at the time of the “Old Metallurgist”. The reason? As informatics was considered by the Soviet ideology as a “capitalist pseudoscience”, modern MS&E work could start to develop ion CEEs only with the advent of fundamental political changes, the levying of embargo, in the nineties. This was not an easy task, as e.g., even patent matters were not considered earlier at all and a clearing-up took a lot of effort, foreign capital influx, factory shutdowns, etc.[1] We had a generation of engineers, who were prevented from travelling, yet with huge personal experience, albeit with a kind of amateurism as seen from the outside. However, they were trained in a special skill: the ability to solve problems individually, by instinct. The author’s experience in the liberated Hungary was not at all negative, though his country enjoyed a certain and relative freedom where earlier international practice was concerned.

The new freedom for the young ones in the nineties was difficult to live with. Scientific, industrial partnership is a matter of trust, of friendship. To build this up is not just a web partner search, but takes time and personal effort, friendly “get-togethers” at conferences, etc. Slowly, however, we are seeing results. Some of them are pseudo-negative, when one considers the probably never-to-return intellectual power but clever science and good industrial politics can improve this. The author’s personal exposure to the establishing of Intel in the US (1969 and thereafter) as part of

[1] The author’s eyes were opened in the eighties, when working as a research associate at Faculty of MS&E of Cornell University (NY).

Table 1. *Interaction and expected influence of present day research in Materials Science and Engineering with different industries*

	Infotechnology	**Energetics**	**Transport**	**Machine and construction industry**	**Chemical, agro-, bio-industry**	**Medical industry**
Semiconductor	Si, SiGe, A+B5, carbon nanotube, graphene, other 2D materials, e.g., MoS_2	Blue LED power electronics, SiC		**Solar cells Revolution of lighting**	Organic semiconductors	Active implants Microfluidics, dose controllers, lab-on-chip
Structural ceramics	Transparent ceramics	Turbines, bearings	Engines, Otto and ("1-2 l") hybrid, electric	engines, tools, hard coatings, robotic machines		Prostheses
Functional ceramics	Sensors, high temp. Superconductors	Fuel cells, High T sensors, batteries, supercapacitors, superconductors		Sensors, nanostructuring	Sensors, actuators.	Neural stimulators
Materials for optics and photonics	Waveguides, "photonic bandgap", metamaterials	Low consumption electronics, LED, laser (GaN),		Monitors	Telecontrol	Artificial sensing organs (eye prosthesesí9
Polymers	low, high k, CD, memory materials, dielectrics	Solar elements, insulators	Corresponding to demands of transportation	Temperature resistant and load tolerable polymers (300-500 km self load), „smart" active materials		Peptides, lipids, „nanomedicine", self-organization and biocompatible, „smart" materi-als, „biomimetics"
	Revolution of lighting: OLED, PLED				Membranes, self-organization, copolymers,	
Metals	Pure metals, Cu, Au, W, Ta, etc.), superconductors	Light composites, metallic foams, „smart" active materials, Special steel materials			nanocomposites	Composites, Prostheses, "smart" active materials
Nanostructured materials	Magnetic , piezo- nanostructures, Quantum computer, energy harvest, graphene	Turbines	Fullerene-like compounds, CN, BN, diamond		Corrosion resistant materials, alloys	**Prostheses, biocompatible, fullerene-like, diamond, biosensors**
			Materials for heavy load and corrosion resistant structural materials, coatings			
Multifunctionals micromachining, MEMS + nano	Adaptive optics	Self-optimizing materials	Smart spacers, brakes, safety	Smart tools, smart houses, buildings	Smart machines, GPS-control	Smart implants, , "smart" artificial sensing organs
	Smart sensors with telecommunication Revolution of sensors and actuators, Metamaterials (negative permeability, cloak for invisibility);					

his Caltech post doctorate, and his involvement in the R&D of Intel's mother company, Fairchild Semiconductors, proves that being part of a big company, clever engineers may pick up enough knowledge to start their own company. Maybe first as a component deliverer. This is what I maintain as a hope for young engineers in CEE countries. [5] [6]

References

[1] Agricola G.: *De re metallica*. Basel, 1556. http://www.gutenberg.org/files/38015/38015-h/38015-h.htm

[2] Moore G.: *Cramming more components onto integrated circuits*. Electronics, 38/8. (1965). http://archive.computerhistory.org/resources/access/text/2017/03/102770822-05-01-acc.pdf

[3] Drexler E. K.: *Engines of creation: The coming era of nanotechnology*. Anchor Books, New-York, 1986. http://e-drexler.com/p/06/00/EOC_Cover.html

[4] Feynman R. P.: *There's plenty of room at the bottom.* Előadás, American Physical Society, Caltech, Pasadena, 1959. december 29. Átírata: http://www.zyvex.com/nanotech/feynman.html (letöltve: 2018. május 15.)

[5] Gyulai J.: *Materials science and its importance in middle and central Europe*. In: Physics and industrial development. Bridging the gap. (Chandrasekhar S. (szerk.)), Wiley Eastern Ltd., New Delhi, 1995. 227–232.

[6] Gyulai J.: *Jedlik vagy Siemens?* Új Magyarország, 3. (1993. június 26.).

Acta Materialia Transylvanica 1/1. (2018) 12–18.
https://doi.org/10.2478/amt-2018-0004
Hungarian: ~~https://doi.org/10.2478/amt-2018-0003,~~
https://doi.org/33923/amt-2018-0003
Corrected: 29.08.2023.

Chemical Durability of Uranium Oxide Containing Glasses

Enikő BITAY[1], Irén KACSÓ[2], Erzsébet VERESS[3]

[1] *Sapientia Hungarian University of Transylvania, Faculty of Technical and Human Sciences, Târgu-Mureş, Romania, ebitay@ms.sapientia.ro*

[2] *National Institute for Research and Development of Isotopic and Molecular Technologies (INCDTIM), Cluj, Romania, iren.kacso@gmail.com*

[3] *Transylvanian Museum Society, Cluj, România, veresserzsebet@gmail.com*

Abstract

ZrO_2 doped Na-Ba-borosilicate glasses suitable as matrix materials for HLW immobilization were synthesized and corrosion behaviour was investigated in different aqueous media. Hydrolytic stability is increased with the doping level until 5 mol %; above this value the glass vitrification tendency is strongly intensified. Unexpectedly, ZrO_2 doping diminished the corrosion stability in 1M HCl solution, and low ZrO_2 content showed a low corrosion resistance in 1M Na_2CO_3 solution also. Doping effect was negligible in case of synthetic seawater. The glass structure is significantly stabilized by the integration of the 30% UO_3 added.

Keywords*: borosilicate glasses, HLW immobilization, corrosion stability.*

1. Introduction

Uranium glasses – uranium oxide (UO_2, UO_3 U3O8) doped oxide glasses – have been available on the market since the 1830s. The small quantity of uranium oxide added to the glass melt initially served only as a glass coloring agent, being used in the piece or small series production of diversely (typically yellow-green) colored, intense green UV fluorescence glass jewels (**Figure 1.**), decorative objects, dinnerware (glasses, bottles), enamels and fine ceramic glaze [1]

Uranium dental porcelain compositions of high esthetic aspect were developed starting from 1920-25, as uranium ions were found to reproduce the broad fluorescence spectrum of natural teeth under daylight as well as under incandescent and UV light illumination, assuring a bright white effect of the artificial teeth (after the 1960s, the uranium content was limited to 0.05 %, and nowadays its use has been discontinued) [2–4].

Figure 1. *Synthetic (glass) radioactive stones. Photo: R. Weldon. [9]*

In the 1930s, uranium glasses started their career as ion-sensitive (pH-sensitive) glass electrode membranes. Uranium oxide added in small quantities to a silicate glass melt significantly improved the hydrolytic stability and the electrical conductivity of the glass, opening up the possibility for development of glass electrodes with better functional parameters and longer working life. Furthermore, it gave rise to much more reliable glass electrodes for general and industrial use; and even biomedical microelectrodes suitable for in vivo monitoring. [5–8].

After 1945, the many and varied medical, industrial, agricultural, academic and scientific applications of the various radioisotopes were developed. The ever increasing use of nuclear power associated with civilian nuclear technologies has led to a rapid increase in radioactive waste as a by-product. The growing number of nuclear weapons and military applications, as well as the gradual destruction of nuclear weapon stockpiles

imposed by existing nuclear disarmament agreements, have also generated lots of active and depleted nuclear waste. Consequently, the environmentally secure long-term storage of radioactive waste is more and more critical. Presently, the preferred high activity (mostly uranium and/or plutonium containing) HLW (High Level Waste) encapsulation materials, besides Synroc-type glass-ceramics, are borosilicate or Fe-aluminophosphate matrix glasses. [10, 11].

Sufficient hydrolytic stability of uranium glasses has been an important requirement since their first commercial use. According to the published experimental data, in deionized water the mean U quantity leached from uranium drinking glasses is 0.052 (max. 0.63) μg L^{-1}, in diluted acetic acid it is 5.9 (max. 30.1) μg L^{-1} and in the case of glazed ceramic tableware the U leached can attain 300000 μg L^{-1} [12].

These data explain why after the 1970s, due to the potential damage to health – particularly from the swallowing U – commercial use of U compounds has been gradually restricted. However, investigations carried out on the stability of uranium glasses today are equally important because the quantity of HLW resulting from the nuclear industry, and the destruction of nuclear warheads (which necessitates environmentally safe long-term disposal options) is a constantly growing problem.

1.1. Uranium oxide containing HLW encapsulating glasses

The most important specific characteristics of the first generation HLW host glasses are their glass forming domain, crystallization properties, corrosion behavior, thermal, mechanical and radiation resistance. At the same time, of course, the economic aspects also have to be considered.

1.1.1. Borosilicate glasses [13–15]

Presently borosilicate glasses are the first choice as nuclear waste material matrices. The matrix glass composition is generally a Na-borosilicate, easily modified by the addition of further glass forming and glass modifying oxides (Al2O3, Li2O, CaO, BaO, ZnO, ZrO2, etc.) in order to optimize certain specific properties. They can integrate a significant amount of actinides (U, Pu) in their structure and are generally able to rapidly dissolve a broad spectrum of radioactive waste of different activities and provenance.

Borosilicate glasses are characterized by large glass-forming interval, and excellent chemical (hydrolytic), thermal and (external and internal) radiation stability.

1.1.2. Phosphate glasses [16]

Phosphate glasses, the second most important HLW hosting glass family, differ in many of their properties compared with the borosilicate glasses.

Thermal stability is poorer, and excepting the iron oxide containing phosphate glasses, the chemical stability is much lower, especially in aqueous media. The melting temperatures and the molten glass viscosity are generally much lower, but this is offset by the high corrosivity of the molten material, which significantly shortens the working life of the melting furnace.

The chemical stability of the newly developed Na-Al-phosphate glasses is in some ways improved: leaching rates in the case of aluminophosphate-HLW and borosilicate-HLW are comparable. In corrosion experiments carried out in aqueous solutions and realistic long-term deposition conditions, the main normalized leached radionuclide quantity of the borosilicate-HLW tested was 0.3·10-6 g/cm2 Cs and 0.2·10-6 g/cm2 Sr daily, comparable with 1.1·10-6 g/cm2 Cs and 0.4·10-6 g/cm2 Sr obtained in the case of the aluminophosphate-HLW. [11]. However, the thermal stability is rather low; glass crystallization and temperatures above 100 ºC significantly affect the hydrolytic stability (in the interim storage facilities temperatures can easily exceed 100 ºC); the glass melt is still very corrosive.

Even if glass-forming properties of the newest Pb-Fe-phosphate glasses are below of those of borosilicates, they are sensibly improved: thermal stability is acceptable; chemical stability is good; the molten material is less corrosive. Matrix glass mixtures melt at (commonly by 100-250 ºC) lower temperatures than the borosilicates (melting temperature ranges at 800-1000 ºC), however for the complete dissolution of the HLW a temperature of at least 1000 ºC is necessary.

By increasing the Fe2O3 content, decreasing the PbO content and adding CaO in the matrix glass mixture, the glasses chemical stability can be improved, especially in aqueous salt solutions.

1.1.3. Rare earth oxide glasses [17, 18]

The composition of the so-called Löffler glass, developed in the 1930s as an optical glass is 10-70% lanthanide oxide, 9-20% Al_2O_3, the remaining part being SiO_2. Lanthanide-borosilicate glasses are derived from the Löffler glass. Due

to the relatively high solubility of U, Pu and Am Löffler-type lanthanide-borosilicate glasses are convenient hosts for the disposal of these elements, nevertheless at present these glasses are without practical importance.

1.1.4. Aluminosilicate glasses [19, 20]

Aluminosilicate glasses could be good HLW host materials as they are capable of integrating 20 V/V% UO_2. The disadvantages are their relatively high melting temperature and relatively high crystallization tendency.

The recently synthesized and studied aluminosilicate glasses are characterized by lower melting temperatures, lower viscosity and significantly higher durability. These being considered, based on the results obtained in the light of new developments, in perspective they could be the first representatives of the second generation HLW hosting glass family.

1.1.5. Sintered glasses [21]

By reason of the difficulties raised by the obtainability of high SiO_2 content quartz glasses, researchers are trying to prepare them by sintering of the sol-gel synthesized starting material. Use of the sintering procedure could reduce the temperature required to obtain and process a good HLW hosting quartz glass by several hundred grades, making it possible at the same time to avoid not only the major energy expenses, but also the loss of the volatile radionuclides (Cs, Ru, Mo, Tc).

The HLW to be disposed is practically permanently integrated in the structure of the host quartz glass. As indicated by the microstructural investigations performed, despite the diffusion of the Cs and Ba nuclides and the chemical reaction of the matrix with the Ce, Nd and Zr nuclides, structural integration of the most part of the waste material in the sintered host takes place by clustering processes, not dissolution.

This paper presents experimental results obtained by investigations of the chemical stability of some HLW hosting sodium-borosilicate glasses.

2. Glasses preparation and characterization

2.1. Synthesis

Matrix glasses (**Table 1**) were prepared by the melt-quench method, without specific thermal treatments.

The thoroughly homogenized mixture of the finely pulverized dry p.a. grade starting components (oxides, carbonates, boric acid) was melted in atmospheric conditions in a platinum crucible, stirring the melt periodically with a platinum rod. The progress of the synthesis was followed by visual examination of sample drops removed at the end of every stirring. At the end of the synthesis the homogeneous glass melt was quenched by pouring the melt onto a 5 mm thick stainless steel plate.

Under the same conditions the 70% matrix glass + 30% UO_3 (9 mol% UO_3) compositions was also melted.

2.2. Investigations performed, results

2.2.1. Hydrolysis of the borosilicate glasses

Borosilicate glasses are solid electrolytes structured in a locally ordered atomic network consisting of Si, B and O atoms forming mostly [$SiO_{4/2}$] and [$BO_{3/2}$] electrically uncharged units and≡SiO^- and/or [≡SiOB≡]$^-$ anions. The negative charges of the anionic units are neutralized by ionically linked neighboring alkaline and alkaline earth cations of differing mobilities. Penetration in the glass bulk of the H^+ ions from the aqueous solutions contacting the compact glass surface is strongly hindered (Na^+ mobility in the quartz glass e.g. is 104 greater than H^+ (H_3O^+) mobility). [22].

Table 1. *The matrix glass compositions*

Glass type	Oxidic composition (mol %)				
	SiO_2	B_2O_3	Na_2O	BaO	ZrO_2
B05Ba	65.00	5.00	25.00	5.00	
B05BaZr1	64.00	5.00	25.00	5.00	1.00
B05BaZr2	63.00	5.00	25.00	5.00	2.00
B05BaZr3	62.00	5.00	25.00	5.00	3.00
B05BaZr4	61.00	5.00	25.00	5.00	4.00
B05BaZr5	60.00	5.00	25.00	5.00	5.00
B10Ba	60.00	10.00	25.00	5.00	
B10BaZr5	57.14	9.52	23.80	4.76	4.76
B15Ba	55.00	15.00	25.00	5.00	

Referring to silicate glasses Baucke [23] conceived several hypotheses which are also valid to borosilicate glasses:

a) Structural cations in the glasses in contact with aqueous electrolytes are influenced by the potential gradient generated by the concentration gradient
b) [SiO]$^-$ and [SiOB]$^-$ type anionic groups of the glass surface belong equally to the glass phase

and the aqueous electrolyte solution in contact with the glass surface and are in equilibrium with the ions existing in electrolyte solution

c) Due to the equilibrium processes after the hydration of the glass surface the hydrolysis of the silicate (borosilicate) glass network occurs (glass corrosion).

Vizes elektrolitoldatban tehát a határfelületi folyamatok következtében a boroszilikátüveg felületi rétege megduzzad (hidratálódik), majd oldódni kezd (korrodálódik, hidrolizál).

Thus, in aqueous electrolyte solutions the surface layer of the borosilicate glass becomes swelled (hydrated), the hydration process being followed by its dissolution (corrosion, hydrolysis).

The corrosion rate and extent is defined by two basic processes [24, 25]:

- ion-exchange controlled diffusion

$$(\equiv Si\text{-}O\text{-}A)_g + H_2O \leftrightarrow (\equiv Si\text{-}O\text{-}H)_g + A\text{-}OH \quad (1)$$

(A – any alkaline cation)

- hydrolysis of the silicate network:

$$\equiv Si\text{-}O\text{-}Si\equiv + H_2O \leftrightarrow 2(\equiv SiOH) \quad (2)$$

The rate of the ion-exchange reaction is defined by the pH-dependent effective diffusion coefficient D_A of the interdiffusion process, and the E^d_A activation energy characterized by an Arrhenius-type temperature dependence (the activation energy of leaching processes is typically ≈ 30–145 kJ/mol)

The alkaline components leaching due to selective dissolution and exchange to hydrated protons (H_3O^+) during the ion-exchange reactions, generates an alkaline ions shortened hydrated glass surface layer. In the following hydrolysis process hydroxyl ions contacting the hydrated glass surface react with the silicate network-resulting silicic acid (H_4SiO_4) which leads to the complete dissolution of the glass network:

$$\equiv Si\text{-}O\text{-}Si\equiv + OH^- \leftrightarrow \equiv SiOH + \equiv Si\text{-}O^- \quad (3)$$

$$\equiv Si\text{-}O\text{-}Si(OH)_3 + OH^- \leftrightarrow \equiv Si\text{-}O^- + (H_4SiO_4)_{aq} \quad (4)$$

$$\equiv Si\text{-}O\text{-}Si(OH)_3 + H_2O \leftrightarrow \equiv Si\text{-}OH + (H_4SiO_4)_{aq} \quad (5)$$

2.2.2. Hydrolytic stability investigations

Corrosion stability of the synthesized matrix glasses and the corresponsive 30% UO_3 containing glasses was determined in different aqueous media: distilled water, acidic solutions, alkaline solutions, and saline solutions corresponding to seawater salinity. In the case of distilled water the method applied was that specified in the ISO 719 standard, in the other cases the properly modified version of the before mentioned method was used.

2.2.2.1. Experimental

Before carrying out determinations, the ground glass samples of controlled particle size were conditioned according to the ISO 719 standard: thorough washing with bi-distilled water, rinsing with p.a. ethanol, drying at 60 °C. The corrosion media used were bi-distilled water and the following solutions, prepared in bi-distilled water solvent and analytical grade reagents: 1M HCl, 1M Na2CO3, and synthetic seawater (**Table 2.**).

Static corrosion experiments were performed on the following ground glass fractions obtained using Retsch laboratory sieving equipment:

– in bi-distilled water: 0,3–0,5 mm
– in 0,1 N HCl solution: 0,5–1,0 mm
– in 0,1 N Na_2CO_3solution: 1,0–1,5 mm
– in synthetic seawater: 1,0–1,5 mm

Samples of 0.5 ± 0.05 g of the proper glass fraction were analytically (± 0.0001 g) transferred in 25 cm^3 volumetric flasks filled to the sign with the corresponding corrosive solution. The prepared open volumetric flasks were kept at 98 °C for 2 hours, then the room-temperature flasks were refilled with the corrosion solution and were homogenized. The samples used for the measurements were taken from these stock solutions.

The mass loss measuring procedures of the usual standards given for glasses in case of acid corrosion (ISO 1776), and corrosion in alkaline and salt solution media (ISO 695) couldn't be applied because of the limited quantity of the glasses, therefore, the leached elements in these cases were determined by ICP-AES spectrometry. ICP-AES method compliance was verified by comparing the experimental results with the ISO 719 method results obtained on the same samples in the case of hydrolytic stability in bi-distilled wa-

Table 2. *Synthetic seawater composition [26]*

Component	Content (g/L)
NaCl	23.9985
Na_2SO_4	4.0111
KCl	0.6986
$NaHCO_3$	0.1722
KBr	0.1000
H_3BO_3	0.0254
NaF	0.0029
$MgCl_2$	5.0290
$CaCl_2$	1.1409
$SrCl_2$	0.0143

ter. Due to the parallelism of the two data series, concordance between the two different methods was considered satisfactory.

2.2.2.2. ISO 719 titrimetric method

Samples taken from the extraction solutions obtained were potentiometrically titrated using 0.01N HCl solution as titrant, pH glass measuring electrode and Ag/AgCl reference electrode. (Standard deviation: 0,1%). Corrosion (hydrolytic) stability is defined by the Na_2O quantity extracted from 1 g glass sample in µg units, and by the consumption of the titrant solution used in mL (**Table 3.**).

2.2.2.3. ICP-AES determinations

ICP-AES measurements were performed on a Jobin-Yvon 24 type sequential ICP-AES spectrometer provided with argon gas of 99.995% purity for the plasma. Determinations were repeated on three parallel samples for every element in the case of every glass, working on the spectral lines presented in **Table 4.**

In order to assure the correctness of the determinations, a five point matrix-identical multi-element calibration was performed in every corrosion medium at five properly chosen concentration levels. The concentration of the standard solutions used in case of the determinations on bi-distilled water extracts were 0.0; 0.5; 1.0; 5.0 and 10.0 ppm for every element (**Figure 2**). Standard deviation of the method was of 1-2%.

In case of the bi-distilled water and the acidic solution extracts the concentration level of the standard solutions and the matrix (the extract) was analogous and the sample solutions to be measured could be used "as is". As part of the metallic ions separated (precipitated) from the seawater and the alkaline standards, in these cases the calibration standards and the measurable samples were previously diluted, applying a dilution ratio of 1:10.

Table 3. *Glass hydrolytic classes (ISO 719)*

V 0,01M HCl mL	Na_2O µg	Hydrolytic class
≤ 0,1	≤ 31	1
0,1–0,2	31–62	2
0,2–0,85	62–264	3
0,85–2,0	264–620	4
2,0–3,5	620–1085	5
≥ 3,5	≥ 1085	> 5

Table 4. *The spectral lines used for ICP- AES de-terminations*

Ele-ment	Ba	B	Si	Na	Zr
λ (nm)	233.527	208.959	212.412	588.995	257.139

2.2.3. Results

All the synthesized glasses, derived from the $65SiO_2 \cdot 5B_2O_3 \cdot 5BaO \cdot 25Na_2O$ [mol %] oxide system, can be arranged in the following two groups:

a) B05Ba (alap); B05BaZr1.....B05Ba5Zr5;

b) B05Ba (alap); B05Ba, B10Ba, B15Ba; in this latter the ZrO_2 doped B10BaZr is included, proven to be the optimal composition.

2.2.3.1. Titrimetric method (ISO 719)

The ISO 719 standard method of hydrolytic stability determination was only applied to the group (b) matrix glasses and their 30% UO_3 doped variants. Titrations were performed on three 5 ml extract samples for every glass sample.

As expected, in the case of similar B_2O_3 content the ZrO_2 addition increases the hydrolytic stability of the Ba-borosilicate glass system. At the same time it can be ascertained that the integration of the UO_3 in the glass network [27, 28] has the effect of stabilization of the glasses, raising their compactness and corrosion stability (**Figure 3**, **Table 5.**).

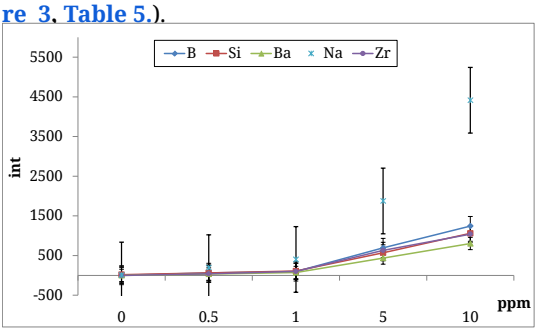

Figure 2. *ICP-AES calibration in bi-distilled water*

Table 5. *Effect of UO_3 integration in the glass network on the hydrolytic stability*

Glass type	Hidrolitikus stability (0.01N HCl, mL)		Density at 20°C (g/cm³)	
	Mátrix	30% UO3	Mátrix	30% UO3
B05Ba	2.25		1.857	
B10Ba	4.50	0.44	2.014	2.183
B10BaZr	2.87	0.14	2.307	2.484
B15Ba	2.35	0.56	2.208	2.424

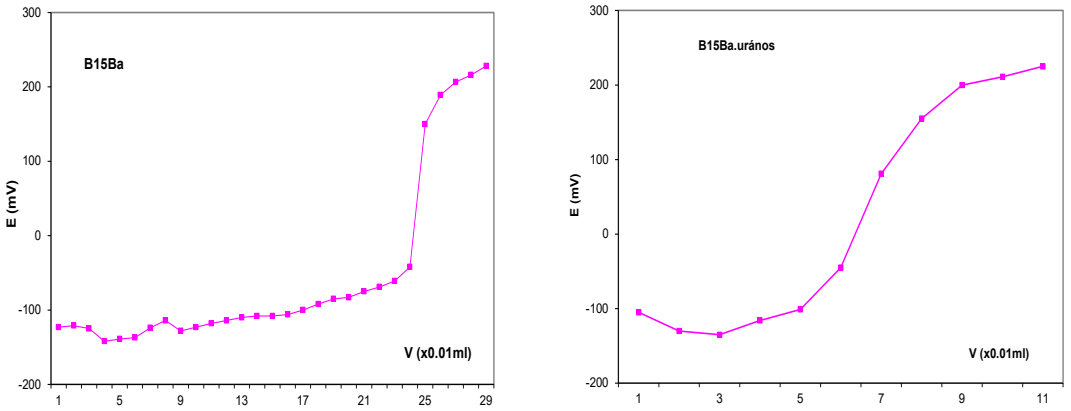

(a) (b)

Figure 3. *Titration curves obtained for B15Ba (a) and (70%) B15Ba·(30%)UO_3 (b)*

Table 6. *Influence of the ZrO_2 integration in the glass network on the corrosion stability vs. different aqueous media*

Glass type	Normalized total extracted oxide quantity µg/g ground glass			
	H_2O	0.1N HCl	0.1N Na_2CO_3	See water
B05Ba	8.88	1.99	3.37	0.69
B05BaZr1	30.15	29.67	9.92	0.42
B05BaZr2	27.66	24.67	2.33	0.31
B05BaZr3	19.98	18.63	3.55	0.47
B05BaZr4	14.93	14.93	5.83	0.36
B05BaZr5	10.91	13.39	2.93	0.42

2.2.3.2. ICP-AES method

Experimental results obtained by the ICP-AES method for the hydrolytic stability (vs. H_2O) and the chemical resistance (vs. acidic, alkaline and saline solutions) of the group (a) matrix glasses is presented in **Table 6**. (Normalized total metal ion quantity extracted in static conditions at 98 ºC). **Table 6** data indicate that at the B05Ba (basic) glass derived ZrO_2 doped glasses the influence of the ZrO_2 network integration [29, 30] on chemical stability of the glasses is observed starting from 2 mol % ZrO_2 added. In order to completely clarify the network stabilization effect tendency in this case, further study is required.

3. Conclusions

Hydrolytic stability of the studied Ba-borosilicate matrix glasses is increased by the B_2O_3 addition starting from 10 mol % B_2O_3 added.

At the same B_2O_3 content ZrO_2 doping increases the hydrolytic stability. The effect is maximal at 5 mol % ZrO_2. Further doping significantly increases the vitrification tendency.

In the case of vitrification of Zr-containing wastes, the fact that ZrO_2 addition decreases the corrosion resistance of borosilicate glasses in acidic media should be taken into account.

UO_3 integration in the glass network increases the chemical stability significantly.

References

[1] Skelcher B. W.: *The big book of vaseline glass*. Schiffer Publishing Ltd., 2002.

[2] El-Meliegy E., van Noort R.: *Development of colour and fluorescence in medical glass ceramics*. In: Glasses and glass ceramics for medical applications. Springer, New York, NY, 2011. 149–164. https://doi.org/10.1007/978-1-4614-1228-1

[3] Thompson D. L.: *Uranium in dental porcelain*. U.S. Department of Health, Education, and Welfare, Public Health Service, Food and Drug Administration, Bureau of Radiological Health, Rockville, MD, 1976. https://www.nrc.gov/docs/ML0322/ML032230109.pdf

[4] Ceylan G., Köprülü H., Kurt M., Basoglu T., Güler A. U., Yapici O.: *Uranium in dental porcelain*. Atatürk Üniversitesi Dis Hekimigli Fakultesi Dergisi, 13/3–14/1. (2003-2004) 18–22. http://dergipark.gov.tr/download/article-file/27627

[5] Trietley H. L.: *Electrochemical transducers*. In Transducers in mechanical and electronic design. CRC Press Marcel Dekker, 1986. 162–175.

[6] Pradel A., Saint Aman E.: *Potentiometric sensors (Ions and dissolved gases)*. In: Chemical and biological microsensors. Applications in liquid media (Szerk.: Fabry P., Fouletier J.), Wiley Online Library, 2013. 81–113. https://doi.org/10.1002/9781118603871.ch4

[7] Koryta J.: *Ion-selective electrodes*. Annual review of materials science, 16/1. (1986) 13–27. https://doi.org/10.1146/annurev.ms.16.080186.000305

[8] Kurzweil P.: *Metal oxides and ion-exchanging surfaces as pH sensors in liquids. State-of-the-art and outlook*. Sensors, 9/6. (2009) 4955–4985. https://doi.org/10.3390/s90604955

[9] Nassau K., Lewand E. A.: *Mildly radioactive rhinestones and synthetic spinel-and-glass triplets*. Gems & Gemology, 25/4. (1989) 232–235. https://www.gia.edu/gems-gemology/winter-1989-radioactive-synthetic-spinel

[10] Donald I. W., Metcalfe B. L., Taylor R. N. J.: *The immobilization of high level radioactive wastes using ceramics and glasses.* Journal of Materials Science, 32/22. (1997) 5851–5887. https://doi.org/10.1023/A:1018646507438

[11] Ojovan M. I., Lee W. E.: *Glassy wasteforms for nuclear waste immobilization.* Metallurgical and Materials Transactions A, 42/4. (2011) 837–851. https://doi.org/10.1007/s11661-010-0525-7

[12] Landa E. R., Councell T. B.: *Leaching of uranium from glass and ceramic foodware and decorative items.* Health Physics, 63/3. (1992) 343–348. https://doi.org/10.1097/00004032-199209000-00012

[13] Hench L. L., Clark D. E., Campbell J.: *High level waste immobilization forms*. Nuclear and Chemical Waste Management, 5/2. (1984) 149–173. https://doi.org/10.1016/0191-815X(84)90045-7

[14] Plodinec M. J.: *Borosilicate glasses for nuclear waste imobilisation.* Glass Technology, 41/6. (2000) 186–192. https://www.ingentaconnect.com/content/sgt/gt/2000/00000041/00000006/4106186

[15] Sengupta P., Kaushik C. P., Dey G. K.: *Immobilization of high level nuclear wastes. The indian scenario*. In: On a sustainable future of the earth's natural resources. (Szerk.: Ramkumar M.), Springer Earth System Sciences, Springer, Berlin, Heidelberg, 2013. 25–51. https://doi.org/10.1007/978-3-642-32917-3_2

[16] Ray D. E., Ray C. S.: *A review of iron phosphate glasses and recommendations for vitrifying Hanford waste* (No. INL/EXT-13-30839). Idaho National Laboratory, Idaho Falls, 2013. https://inldigitallibrary.inl.gov/sites/sti/sti/6013244.pdf (letöltve: 2018. május 15.)

[17] Plodinec M. J.: *Development of glass compositions for immobilization of Savannah river plant waste.* In: Scientific basis for nuclear waste management (Szerk.: McCarthy G.J.), Springer, 1979. 31–35. https://www.osti.gov/servlets/purl/6227870

[18] Wicks G. G., McKibben J. M., Plodinec M. J., Ramsey W. G.: *SRS vitrification studies in support of the US program for disposition of excess plutonium.* In: Disposal of weapon plutonium–Approaches and prospects. NATO Advanced Science Institute Series, Subseries, 1, (Szerk.: Merz E. R., Walter C. E.), Kluwer Academic Publishers, Dordrecht/Boston/London, 1996. 143–154.

[19] Tan S., Ojovan M. I., Hyatt N. C., Hand R. J.: *MoO_3 incorporation in magnesium aluminosilicate glasses*. Journal of Nuclear Materials, 458. (2015) 335–342. https://doi.org/10.1016/j.jnucmat.2014.11.069

[20] Ahmadzadeh M., Marcial J., McCloy J: *Crystallization of ironcontaining sodium aluminosilicate glasses in the $NaAlSiO_4$–$NaFeSiO_4$ join*. Journal of Geophysical Research: Solid Earth, 122/4. (2017) 2504–2524. https://doi.org/10.1002/2016JB013661

[21] Woignier T., Primera J., Reynes J: *Nanoporous glasses for nuclear waste containment*. Journal of Nanomaterials, 2016. (2016) 1–10. https://doi.org/10.1155/2016/4043632

[22] Doremus R.H.: *Diffusion of reactive molecules in solids and melts*. Wiley, 2002.

[23] Baucke F. G. K.: *The origin of the glass electrode response.* In: Glass... Current Issues (Szerk.: Wright A.F., Dupuy J.) NATO ASI Series (Series E: Applied Sciences), 92. Springer, Dordrecht, 1985. 481–505. https://doi.org/10.1007/978-94-009-5107-5_40

[24] Veress E., Hopârtean E., Savici C., Bokor A.: *Sticle electrodice de pH. I. Elaborarea si caracterizarea fizică a unor sticle litice*. Revista de Chimie, (București), 38. (1987) 495–499.

[25] Moimas L., De Rosa G., Sergo V., Schmid C.: *Bioactive porous scaffolds for tissue engineering applications: Investigation on the degradation process by Raman spectroscopy and scanning electron microscopy.* Journal of Applied Biomaterials and Biomechanics, 4/2. (2006) 102–109. https://doi.org/10.1177/228080000600400205

[26] Millero F. J.: *Chemical oceanography*, CRC Press, 1996.

[27] Collier N., Harrison M., Brogden M., Hanson B: *Release of uranium from candidate wasteforms*. Mineralogical Magazine, 76/8. (2012) 2939–2948. https://doi.org/10.1180/minmag.2012.076.8.09

[28] Fábián M., Sváb E., Zimmermann M.: *Structure study of new uranium loaded borosilicate glasses*. Journal of Non-Crystalline Solids, 380. (2013) 71–77. https://doi.org/10.1016/j.jnoncrysol.2013.09.004

[29] Calas G., Galoisy L., Cormier L., Ferlat G., Lelong G.: *The structural properties of cations in nuclear glasses*. Procedia Materials Science, 7. (2014) 23–31. https://doi.org/10.1016/j.mspro.2014.10.005

[30] Hopf J., Kerisit S. N., Angeli F., Charpentier T., Icenhower J. P., McGrail B. P., Windisch C. F., Burton S. D., Pierce E. M.: *Glass–water interaction: Effect of high-valence cations on glass structure and chemical durability.* Geochimica et Cosmochimica Acta, 181. (2016) 54-71. https://doi.org/10.1016/j.gca.2016.02.023

Acta Materialia Transylvanica 1/1. (2018) 19–25.
https://doi.org/10.2478/amt-2018-0006,
Hungarian: ~~https://doi.org/10.2478/amt-2018-0005,~~
https://doi.org/10.33923/amt-2018-0005
Corrected: 29.08.2023.

A New Method for Determining the Pullability of Composite Reinforcing Ceramic Fibres

János DOBRÁNSZKY,[1] Enikő BITAY[2]

[1] *MTA–BME Research Group for Composite Science, Budapest, Hungary, dobranszky.janos@eik.bme.hu*

[2] *Sapientia Hungarian University of Transylvania, Faculty of Technical and Human Sciences, Târgu-Mureş, Romania, ebitay@ms.sapientia.ro*

Abstract

A unique method for producing aluminium matrix composite wires is the Blücher's process, i.e. continuous gas-pressure infiltration. An essential condition of the process is that the fibre roving of the reinforcing fibres can be pulled across the orifices of the gas-pressure system with the least damage. The article describes a new test procedure that is capable of characterizing this essential functional property of the ceramic reinforcing fibres in a manner comparable and quantitative.

Keywords*: metal matrix composite, reinforcing fibre, continuous gas-pressure infiltration*

1. Introduction

Since the early 2000s, a composite core has been used as a reinforcement in high-tension electrical conductors instead of a steel core. The advantages of the composite core are the lower coefficient of thermal expansion and the higher specific strength. The composite core reinforced electric conductors of overhead transmission lines have gained ground among cables that have very low sag even at high current (HCHS core). The leading type is the so-called aluminum conductor composite core (ACCC) cable. In this cable the reinforcing core is made of carbon fiber re-enforced polymer matrix composite. In another important type of low sag electric conductors (ACCR; aluminum conductor composite reinforced), steel core wires are replaced by aluminum matrix ceramic fiber reinforced composite wires. The permissible maximum temperature of this exceeds that of the ACCC cables. In fact, only two solutions were successful in producing aluminum matrix composite wires: the first one is the Blücher process [1] which is based on continuous gas-pressure infiltration [2]. only this second is used on an industrial scale. As a key operation of the Blücher process, the fiber roving must be pulled across the gas-pressure system [3] containing the melt. In a fiber roving, more tows (thus untwisted fiber bundles) are combined.

The pullability of the reinforcing fibers as a functional property has not been studied so far. This is because using continuous gas-pressure infiltration is only possible for the Blücher process to produce composite wires, and research activities using this method have acknowledged that some types of reinforcing fibers cannot be used. For almost 15 years, a successful series of experiments on the production of carbon fiber reinforced composite wires[4], could not be reproduced, and the purely aluminum-oxide ceramic fibers (e.g. Nextel 610) have also been considered to be unsuitable for continuous gas-pressure infiltration.

The pullability as a requirement for fibers gained importance when we started researching the applicability of the Dialed carbon fiber and CeraFib 99 ceramic fiber as a composite reinforcing material. This article describes the method developed for determining the pullability of reinforcing fibers..

2. The reinforcing fibers of the composite wire

Only those materials in which the reinforcing material and the metallic matrix are separated during the entire manufacturing process [5, 6]. are called metal matrix composites. This is consistent with Ashby's definition: composites – that are, composite materials – are formed by composing two materials that are solids themselves and when the cohesive matrix is metallic then it is a metallic matrix composite [7].

When manufacturing aluminum matrix composite wires with continuous infiltration, the fiber roving has to be infiltrated in its full cross-section with the molten metal [8]. Research activities for the provision of conditions for spontaneous infiltration[9] were unsuccessful in terms of practical applicability, and although thousands of meters of composite wires were produced on the laboratory equipment, the Blücher process did not reach industrial application; this was only managed with a much slower, ultrasonic process [2].

The aluminum matrix composite wires are manufactured by means of the Blücher process, by pulling across a special three-element orifice system. The diameter of the orifices matches the fiber roving and the diameter of the composite wire to be produced. The fiber roving arrives at the inlet orifice under the pressurized chamber containing the melt, and their impregnation with the molten metal begins here.

During the pulling across, the fiber roving is compressed at the entrance of the inlet orifice, the filaments contacting the orifice wall are strongly rubbed against the orifice wall, and there may be various mechanical effects between the fibers inside the fiber roving which cause the fibers to be fractured (**Figure 1**).

Experience has shown that even the filaments of easy-to-handle oxide ceramic fiber roving become fragmented within (**Figure 2**). The roving

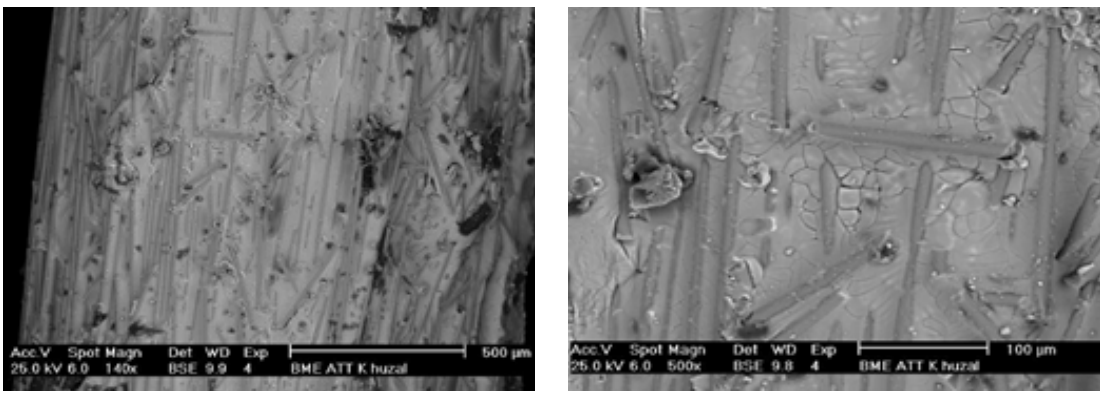

Figure 1. *Total width of the surface of the aluminum matrix composite wire (above) and a detailed view (below); it can be seen clearly how the fibers on the surface are fractured*

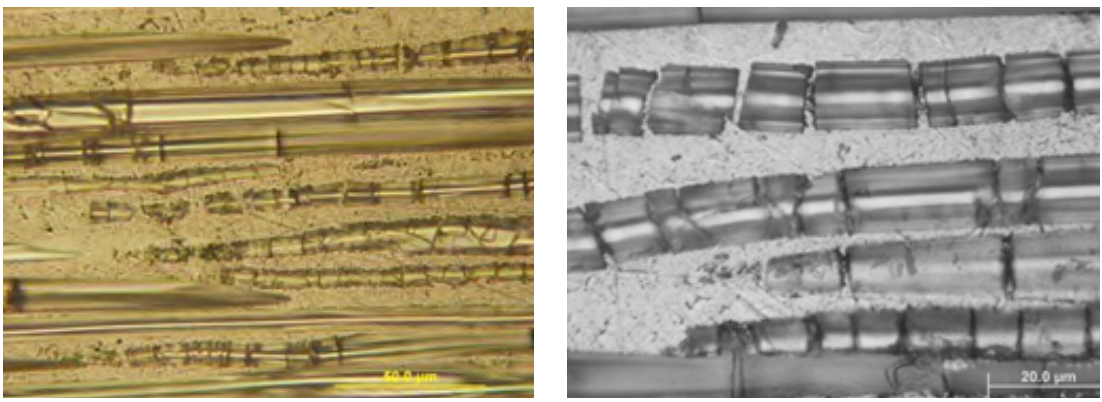

Figure 2. *Wire fractures inside the composite wire; polished longitudinal section of the composite wire on an optical micrograph*

Figure 3. *Fluffing of the carbon fiber tow at the en-trance of the inlet orifice made of graphite*

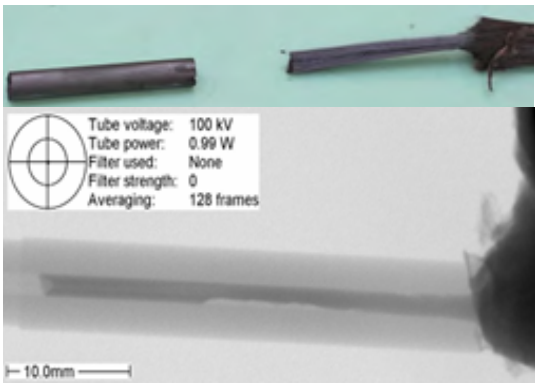

Figure 4. *The optical and X-ray microscope image of the carbon fiber tow torn in the orifice*

Figure 5. *CeraFib 99 fiber roving fed into the inlet orifice, prepared for pulling across*

becomes fluffy, clogs the entrance of the orifice (**Figure 3**), and at the end pulls the orifice off or breaks it. **Figure 3** shows the formation of fluffs at the 1.6 mm diameter graphite orifice when pulling across the Dialed K63712 carbon fiber tow (the tow is an untwisted fiber bundle of numerous filaments), after burning off the sizing. The drawnin fiber pieces are caught by the central orifice, the entrance of which is immersed in the melt and gradually clogs the entrance (**Figure 4**), causing the roving to break.

Typically, the carbon fibers are characterized by fluffing, and when pulling the oxide ceramic fibers (**Figure 5**), the separation of the filaments from the roving is typical with breaking of the whole roving in the inlet or central orifice (**Figure 6**).

3. Experiments and tests

It is clear from the foregoing that the critical point of the production of composite wires by continuous gas-pressure infiltration is the conditions of pulling the fiber roving across, which

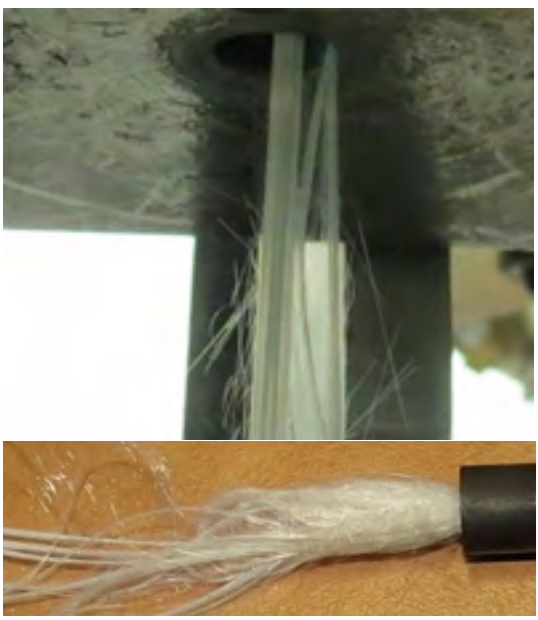

Figure 6. *The CeraFib 99 fiber roving in the process of tearing before the inlet orifice and then torn apart*

all together can be called pullability. Since an inadequate pullability in each case ends in the breaking of the fiber tow – or the whole fiber roving when more tows are used–, it may seem obvious that pullability could be characterized by some strength characteristic of ceramic fibers. However, neither the strength, nor the specific modulus [10–11] provided by the manufacturers suffice, because they say nothing about the breaking behavior of ceramic fibers due to shearing or bending load. For filaments, surface roughness (**Figure 7**) is a sensitive feature, but not for the fiber roving, because as it is pulled across, the pulling system simultaneously moves bunches of thousands of filaments in a fiber roving.

The Al99.5+CeraFib composite wire production process consisted of pulling across a fiber roving comprising approximately 4000 filaments, consisting of 5 fiber tows (**Figure 8**).

In our earlier research it was found that the single-component (e.g. Al2O3) oxide ceramic or carbon fiber bundles are very fragile. The pullability of single-component fibers can be so bad that during the 20 years of the active use of the Blücher

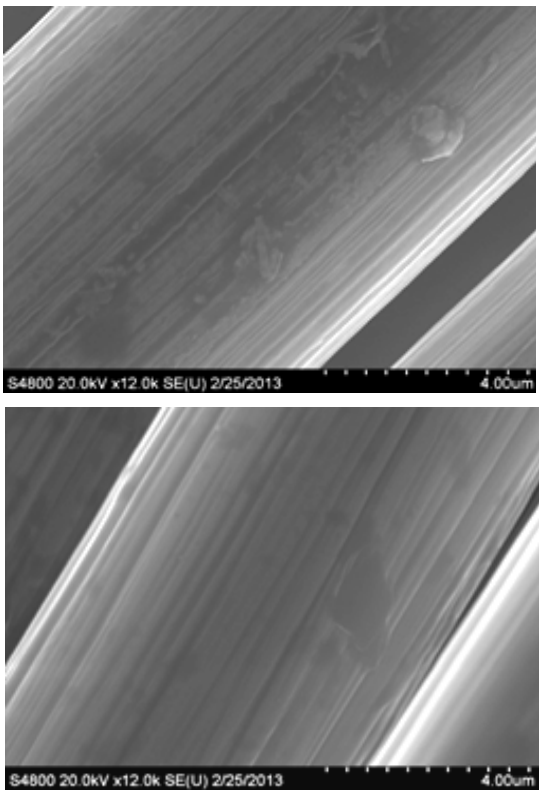

Figure 7. *Surface of filaments; a) Dialed K6372 carbon fiber, b) Zoltek carbon fiberl*

Figure 8. *Pulling across the fiber roving of five tows in the Blücher process*

process (until the end of 2014), no real amount of composite wire was produced from pure oxide ceramic fibers (e.g. Nextel 610), and only one experimental series involving carbon fibers was really effective. In contrast, manufacturing from reinforcing fibers containing mullite and amorphous silica (e.g. Nextel 440) worked with adequate stability to meet the industrial requirements.

For a long time, all this has been explained by the wettability problems, so research efforts have also focused on improving wetting. However, when we started to manufacture Dialed carbon fiber reinforced composite wires, the results of the 'dry' (without molten metal, at room temperature) pulling experiments performed during the development of the inlet orifice revealed that the biggest obstacle was not the weak wetting but the fragmentation and fluffing of the fiber roving. As a result of this discovery, the entire gas-pressure system was completely transformed. In this major design, manufacturing, experimental and material testing work, our excellent post-graduate students played a key role: Péter Törzsök and Károly Tihanyi. Thanks to their extraordinary work, the problem of manufacturing carbon fiber reinforced aluminum matrix composite wires has been solved, and 15 years after the first and only successful series of experiments [4] at Northeastern University (Boston, MA, USA), we managed to repeat it in Budapest [12].

An important element of the solution was to discover the pullability characteristics of the fiber roving and to carry out the appropriate development work to ensure the required pullability (these results have not been published yet).

To characterize the pullability of fiber tows or roving, we developed a testing procedure: the so-called TPTK test. The essence of this is that a loop formed from the fiber bundle is drawn onto the edge of a tool with a polished surface, by uniformly pulling its two branches; the typical dimensions of the tool are shown in **Figure 9** and the test arrangement is shown in **Figure 10**.

Figure 11 – the TPTK diagram – shows the change of tensile force on two types of fiber tow. During drawing, the filaments and the fiber tow itself break at the forced bending angle and bending radius. We look for the greatest force; this is

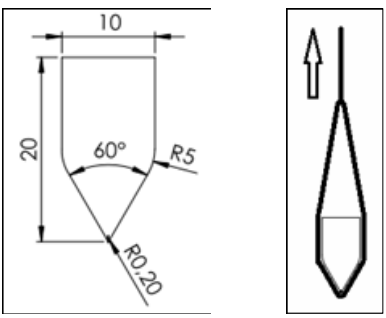

Figure 9. *The tool developed for testing pullability and the outline of the TPTK test*

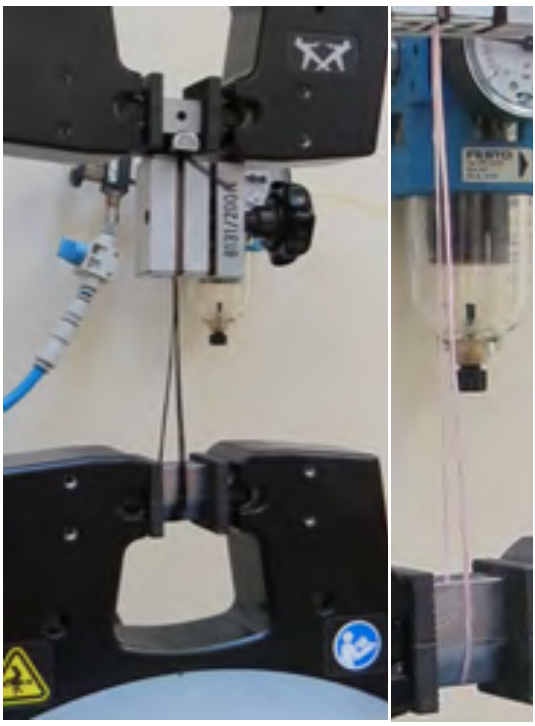

Figure 10. *Mounting the tool developed for testing pullability in the tensile testing machine, using different fiber bundles as an exam-ple*

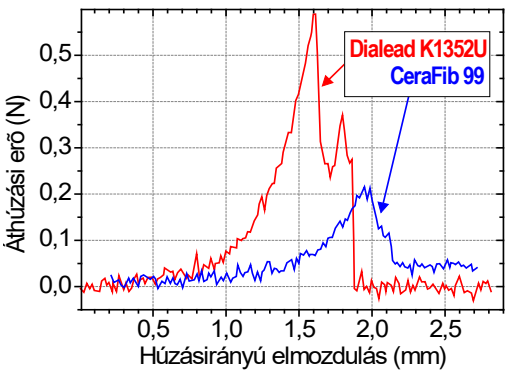

Figure 11. *TPTK diagram of two types of reinforcing fiber*

the TPTK factor that represents a numerical characteristic of pullability.

Table 1. shows the max. force, namely the TPTK factor, characteristic of the pullability for six different reinforcing fibers.

Table 1. *Test data of six reinforcing fibers*

Fiber type	Number of filaments	F_{max} (N)
Tyranno TY-S1A04PX	400	5,11
Tyranno TY-S1A04PX	400	5,05
Tyranno TY-S1A04PX	400	4,06
Dialead K1352U	2000	0,59
Dialead K1352U	2000	0,50
Dialead K1352U	2000	0,59
Dialead K63712	12 000	1,93
Dialead K63712	12 000	1,31
Dialead K63712	12 000	1,85
CeraFib99	468	0,21
CeraFib99	468	0,21
CeraFib99	468	0,17
CeraFib99	468	0,22
Nextel 440	750	2,49
Nextel 440	750	3,51
Nextel 440	750	2,49
Nextel 610	400	0,91
Nextel 610	400	0,83
Nextel 610	400	0,97

4. Evaluating the results

The TPTK diagram, of course, can be evaluated along a wide variety of alignment principles, in which the various features of the filaments – e.g. the number and cross-section of the filaments, the condition of the surface coating of the fiber tow, etc. – can be incorporated, but our experience shows that the maximum value of the pulling force measured during the TPTK test is perfectly suitable for characterizing pullability.

However, we believe that using the TPTK test could provide meaningful information not only for a tow, but also for more tows containing fiber roving, and also for individual filaments. The latter requires a measuring system such as the three-point bending test of the filaments [13] or the filament damage mechanisms due to slip and kink [14, 15].

Generally, in the manufacture of composite wires, depending on the wire diameter and the number of filaments of the tow, 5 to 20 tows must be combined in a fiber roving and fed across the inlet orifice into the gas-pressure system.

During our many years of research, we have found that the increase of the number of combined tows (e.g. Nextel 440) in terms of well pullable reinforcing fibers has no significant effect on pullability. At the same time, in the case of very fragile fibers, pullability is considerably deteriorated by the increase in the number of tows. Even when using up carbon fibers, the pullability of the fiber roving is deteriorated when the diameter of the composite wire requires the introduction and pulling across of more than one tow.

For this reason, we have evaluated the results of TPTK tests based on breakage of the fiber loops, that the force measured during the test is very appropriate indeed for the characterization of the pullability. Thus, the necessarily different tensions when combining multiple tows do not cause any disruptions.

5. Conclusions

Based on the results of the above-mentioned research work and its evaluation, we regard the following conclusions as important to emphasize.

In the production of aluminum matrix composite wires by the Blücher process, the pullability of the reinforcing fibers shall be considered to be a basic functional characteristic. The technical meaning of pullability is that the fiber roving can be pulled through the orifices of the gas-pressure system, especially in the inlet orifice, without fluffing and breaking of fibers causing fracture of the whole fiber roving.

A new test procedure was described for the characterization of pullability, which is based on a bending-pulling-shearing load of the closed loop formed from a piece of fiber tow under forced conditions, until full breakage occurs. For the quantitative characterization of pullability, the TPTK factor was introduced, which is the same as the maximum force measurable during the test.

Based on the pull-across experiments of the reinforcing fibers and the experiments on the production of composite wires as well as the TPTK tests, it can be concluded that the production of composite wires by the Blücher process can only be successful if the TPTK factor of the selected reinforcing fiber is greater than 1. Accordingly, pure oxide ceramic fiber and carbon fiber tows with a low number of filaments should not be used.

Acknowledgments

Among the authors, Enikő Bitay was supported in her research work by the MTA Domus Hungarica Grant Program.

References

[1] Blucher J.T., Narusawa U., Katsumata M., Nemeth A.: *Continuous manufacturing of fiber-reinforced metal matrix composite wires – technology and product characteristics*. Composites Part A: Applied Science and Manufacturing 32/12. (2001) 1759–1766. https://doi.org/10.1016/S1359-835X(01)00024-0

[2] Matsunaga T., Ogata K., Hatayama T., Shinozaki K., Yoshida M.: *Effect of acoustic cavitation on ease of infiltration of molten aluminum alloys into carbon fiber bundles using ultrasonic infiltration method.* Composites Part A: Applied Science and Manufacturing, 38/3. (2007) 771–778. https://doi.org/10.1016/j.compositesa.2006.09.003

[3] Nadler J. H., Isaacs J. A., Kowalski G. J.: *Hydrodynamic modeling of a continuous metal matrix composite fabrication process as a cylindrical array.* Materials Science & Engineering: A, 297/1–2. (2001) 132–137. https://doi.org/10.1016/S0921-5093(00)01266-1

[4] Doktor M.: *Production and characterization of continuous fiber reinforced aluminum wires.* PhD-értekezés, Technische Universität Wien, Institut für Werkstoffkunde und Materialprüfung (2000).

[5] Miracle D. B.: *Metal matrix composites – From science to technological significance*. Composite Science and Technology, 65/15–16. (2005) 2526–2540. https://doi.org/10.1016/j.compscitech.2005.05.027

[6] Evans A, Marchi CS, Mortensen A: *Metal matrix composites in industry: an introduction and a survey*. Kluwer Academic Publishers, Dordrecht, 2003.

[7] Ashby M., Sherdiff H., Cebon D.: *Materials, engineering, science, processing and design.* Butterworth-Heinemann, Oxford, 2007.

[8] Michaud V., Mortensen A.: *Infiltration processing of fibre reinforced composites: goveerning phenomena.* Composites Part A: Applied Science and Manufacturing, 32/8. (2001) 981–996. https://doi.org/10.1016/S1359-835X(01)00015-X

[9] Margueritat-Regenet C.: *Elaboration et caractérisation de fils composites C/Al. Infiltration spontanée et continue par activation chimique du mouillage.* Thèse de doctorat, Ecole nationale supérieure des mines, Paris, 2002. https://hal.archives-ouvertes.fr/tel-00005642/

[10] *High-Performance structural fibers for advanced polymer matrix composites*. National Research Council, The National Academies Press, Washington, D.C., 2005. https://doi.org/10.17226/11268

[11] Ashbee K. H .G.: *Fundamental principles of fiber reinforced composites.* Second Edition. Technomic Publishing Company, Lancaster, 1993.

[12] Tihanyi K: *Fémmátrixú hibrid anyagok gyártása*. Diplomamunka. BME Anyagtudomány és Technológia Tanszék, 2013.

[13] Steinmann W., Saelhoff A. K.: *Essential properties of fibres for composite applications.* In: Fibrous and textile materials for composite applications. Textile Science and Clothing Technology (Szerk: Rana, S., Fangueiro, R.), Springer, Singapore, 2016. 39–73. https://doi.org/10.1007/978-981-10-0234-2_2

[14] Clawson J. K.: *Structure and defects in high-performance aramid fibers*. Master Thesis, University of Illinois, Urbana, 2013. http://hdl.handle.net/2142/46888

[15] Leal A. A., Deitzel J. M., Gillespie J. W.: *Compressive strength analysis for high performance fibers with different modulus in tension and compression.* Journal of Composite Materials, 43/6. (2009) 661–674. https://doi.org/10.1177/0021998308088589

Acta Materialia Transylvanica 1/1. (2018) 26–30.
https://doi.org/10.2478/amt-2018-0008
Hungarian: ~~https://doi.org/10.2478/amt-2018-0007,~~
https://doi.org/10.33923/amt-2018-0007
Corrected: 29.08.2023.

Heat Treatment Effect on Lath Martensite

Enikő Réka FÁBIÁN,[1] Áron KÓTAI[2]

[1] *Óbuda University, Donát Bánki Faculty of Mechanical and Safety Engineering, Department of Materials Technology, Budapest, Hungary, fabian.reka@bgk.uni-obuda.hu*

[2] *Budapest University of Technology and Economics, Department of Materials Science and Engineering, Budapest, Hungary, aron.kotai@gmail.com*

Abstract

During our investigation lath martensite was produced in low carbon steels by austenitization at 1200 °C/20 min, and the cooling of samples in ice water. The samples were tempered at a range of temperatures. The tempering effects on microstructure and on mechanical proprieties were investigated. Some samples with lath martensite microstructure were cold rolled and heat treated at different temperatures. Recrystallization was observed after heat treatment at 600-700 °C.

Keywords*: low carbon steel, lath martensite, heat treatment.*

1. Introduction

Lath martensite in steel shows a hierarchical microstructure consisting of packets, blocks, sub-blocks, and laths. The prior austenite grain is divided into packets that consist of blocks. These blocks in a packet have the same habit plane. The packet is further divided into platelike blocks, which consist of laths with a similar crystal orientation. Lath martensite can be formed in low carbon steel.

It was found [1] that the martensite in the low carbon steels is predominantly lath martensite (under 0.3%wt%C) and plate martensite appears above 0.6 wt%C [2]. The morphology and crystallography of lath martensite has been studied by many researchers in recent years [3-5].

2. Materials and testing

As the first step in our experiment, the lath martensitic microstructure was created in low carbon unalloyed steel (C = 0.15%, Mn = 1.43%, Si = 0.29%). It has been found in the literature that lath martensite can be formed in low-carbon steels by intensive quenching after austenitization at high temperatures. According to our experiments, the higher austenitization temperature supports the more secure formation of the lath martensitic microstructure. The sizes of laths in sub-blocks and blocks are larger and more characteristic after austenitization at 1200°C, than at lower temperatures (**Figure 1-2**).

For our experiments, the lath martensitic microstructures were prepared by austenitization of samples at 1200 °C for 20 minutes and then cooled in ice water.

The properties of lath martensite created in non-alloyed low carbon steel were investigated after heat treatment at different temperatures. For this reason the samples were tempered at 200 °C, 300 °C, 400 °C, 500 °C, 600 °C and 700 °C for 20 minutes, To study exactly the heat treatment effects, the microstructure of the samples was frozen by water cooling.

Impact tests according to MSZ EN ISO 148-3: 2009 on a Charpy impactor were carried out. The tensile tests according to MSZ EN ISO 6892-1: 2016 by Heckert Tiratest 2300 tensile machine were studied. The crossover velocity was 1.5 mm / min. The hardness of the samples was measured using a KB Prüftechnik KB 250 BVRZ type universal hardness tester, and Vickers hardness measure-

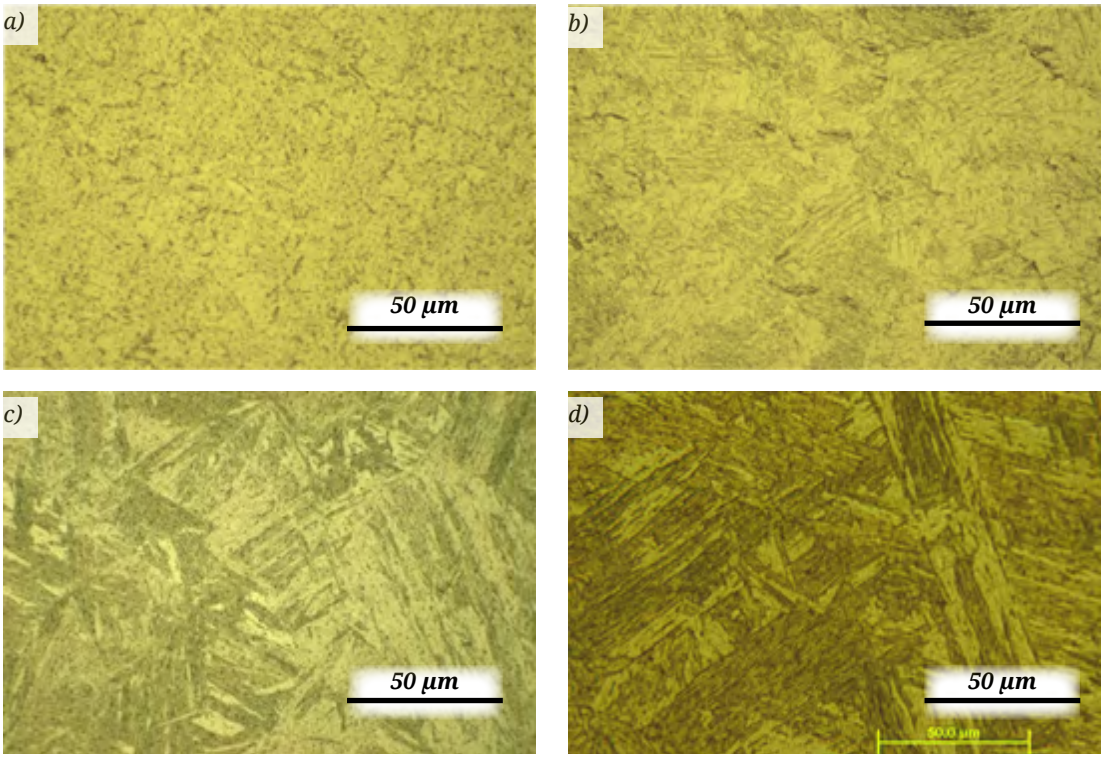

Figure 1. *The effects of austenitization tempera-tures on the microstructure a) T_{aust} = 900 °C; b) T_{aust} = 1000 °C; c) T_{aust} = 1100 °C d) T_{aust} = 1200 °C*

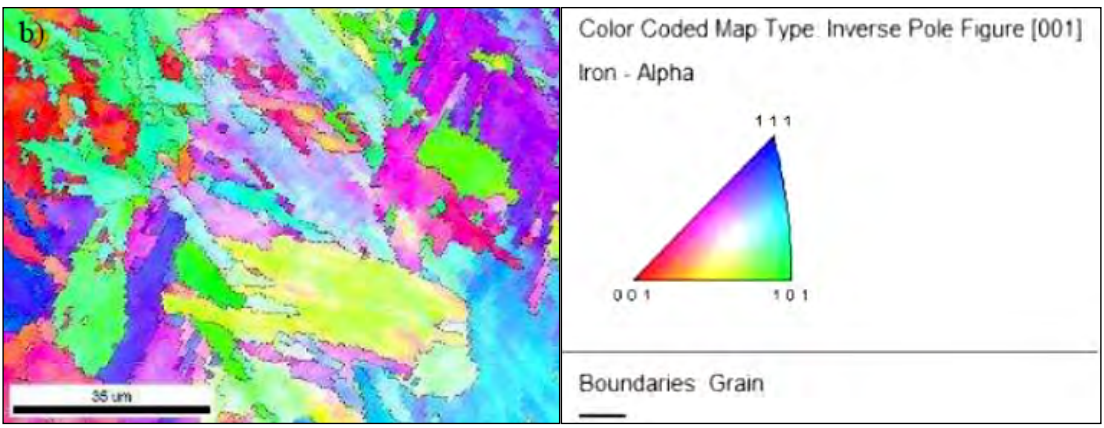

Figure 2. *Orientation map of quenched samples after austenitization at 1200 °C.*

ment. The microstructures of the samples were studied with an Olympus PMG3 light microscope. Investigation of the orientation of the grains, and the small and large angle grain boundaries were achieved by electron diffraction (EBSD) on a Philips XL 30 electron microscope.

Our examinations were extended to examine the effect of cold deformation and subsequent heat treatments. Therefore, 10×10×55 mm samples were rolled on a duo cylinder stand, and after each formulation we studied the effect of post-treatment temperatures. The post heat treatment conditions were similar to heat treatments applied to undeformed samples.

3. Results

As can be seen from Charpy's impact tests, the toughness of the lath martensite after tempering between 200-400 ° C is very small, under 50 J. Increasing the tempering temperature increases the toughness. After tempering at 700 ° C, the toughness of the material was better than that of the normalized base material (**Figure 3**).

Tensile tests (**Figure 4**) showed that elongation at rupture of sample quenched (with lath martensitic microstructure) slightly exceeded 10%. Although the elongation at rupture generally increases with the tempering temperature, when the tempering temperature is 400° C the value is the lowest (between the all measured values is the minimum). Although the toughness of the samples tempered at 700 ° C/ 20 minutes was higher than that of the normalized samples, the elongations at ruptures remain lower than the tensile test specimens in normalized states.

The relationship between the tempering temperature and the tensile strength is confirmed by the tests results The quenching achieved tensile strength (800 MPa), the decreasing of the tensile strength is caused by the 500 °C or higher temperature tempering. The character of lath martensite could be observed in the microstructure after tempering at 700 °C (**Figure 5**).

Cold rolling of the LM material indicated that the material hardened during forming (**Figure 6**) but no cracks occurred even after 86% deformation (535HV10). Further deformations were limited by the 55HRC hardness of the rolling mill cylinders.

Studies carried out after several deformations and heat treatment at various temperatures show that even after extensive deformation, a considerable amount of heat is needed for the recrystallization of unalloyed low carbon with lath martensitic microstructure. While after 62% deformation and heat treatment at 500 °C/ 20 min, by optical microscope we could not observe signs of recrystallization (**Figure 7**), studying the samples by EBSD method at high resolution, in image-quality maps it was possible to distinguish dislocation-free sub-grain centre and dense dislocation network at the sub-grain boundaries (**Figure 8**). On the orientation map it resembled an anisotropic appearance of material.

The hardness of the samples which were deformed more than 30% and heat treated at 600-700 °C become less than 200HV10, in these samples - in image-quality maps, a recrystallized equiaxed microstructure can be observed (even if the grain size is different after 20 minutes of heat treatment at 700 °C) (**Figure 9**).

4. Conclusions

The lath martensitic microstructure in low carbon unalloyed steel has very good deformability and is very stable even at high temperatures.

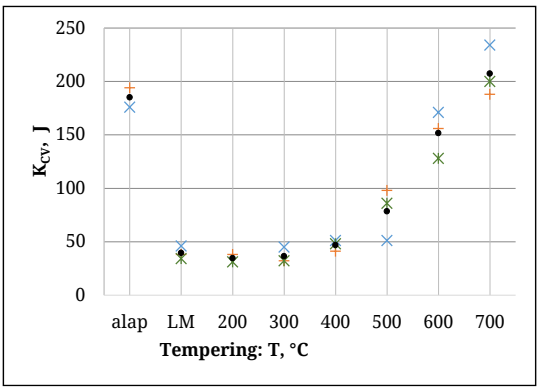

Figure 3. *Tempering effect on impact energy (bm= basic normalized structure, LM= lath martensitic structure)*

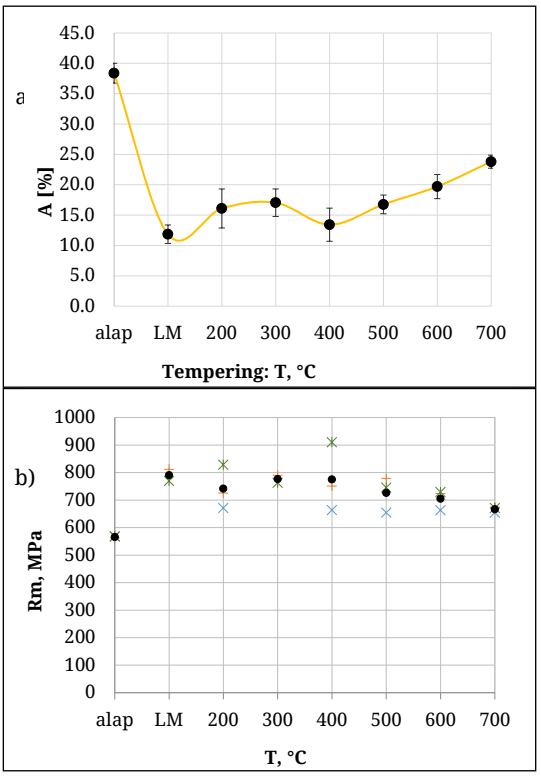

Figure 4. *Tempering effects on elongation at rupture (a) and on tensile strength (b)*

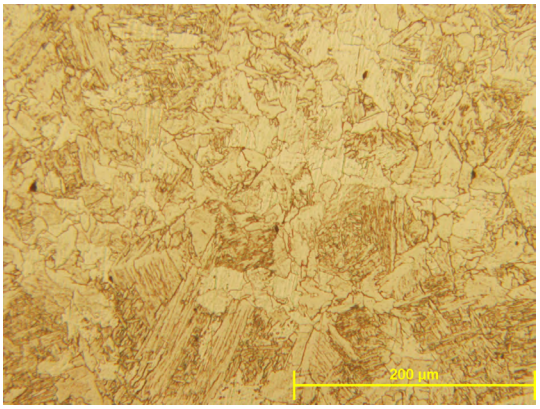

Figure 5. *Microstructure of the LM sample tempered at 700 °C*

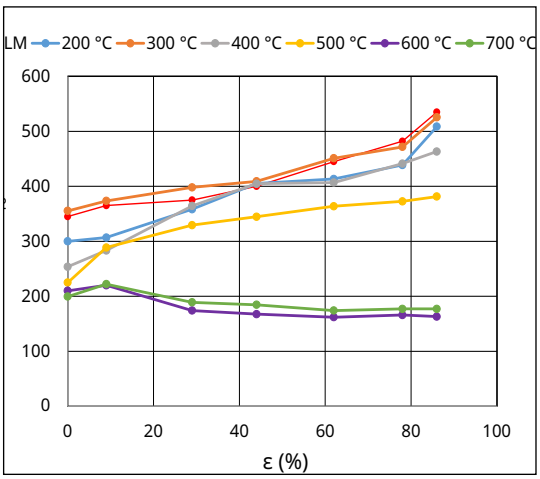

Figure 6. *Cold rolling and tempering effects on hardness of samples with lath martensitic microstructure*

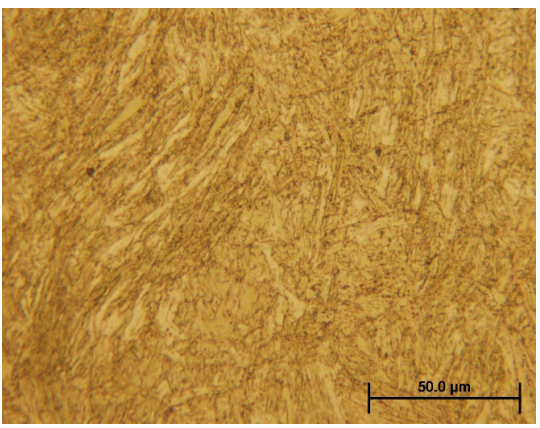

Figure 7. *Microstructure of sample deformed ε=62% and tempered at 500 °C*

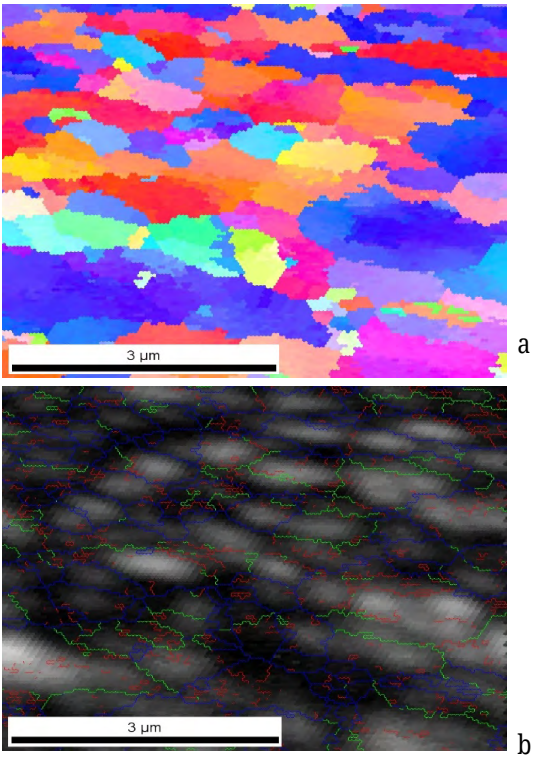

Figure 8. *EBSD images, ε=44%, T=500°C, N=10000x. a) Pole figure map b) Image quality map*

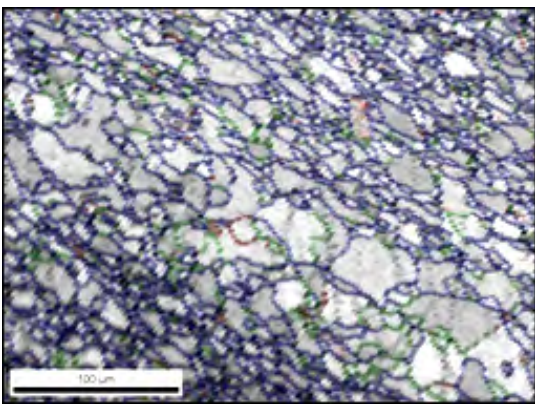

Figure 9. *Image quality map at sample, 86%, T=700 °C*

Acknowledgments

The authors wish to express their thanks for the financial support given by the project EFOP-3.6.1-16-2016-00010.

References

[1] Stormvinter A., Hedström P., Borgenstam A.: *Investigation of lath and plate martensite in a carbon steel.* Solid State Phenomena, 172–174. (2011) 61–66. https://doi.org/10.4028/www.scientific.net/SSP.172-174.61

[2] Sandvik B. P. J., Wayman C. M.: *Crystallography and substructure of lath martensite formed in carbon steels*. Metallography, 16/2. (1983) 199–227. https://doi.org/10.1016/0026-0800(83)90005-8

[3] Kelly P. M.: *Crystallography of lath martensite in steels.* Materials Transactions, JIM (Japan), 33/3. (1992) 235–242. https://doi.org/10.2320/matertrans1989.33.235

[4] Morito S., Tanaka H., Konishi R., Furuhara T., Maki T.: *The morphology and crystallography of lath martensite in Fe-C alloys*. Acta Materialia, 51/6. (2003) 1789–1799. https://doi.org/10.1016/S1359-6454(02)00577-3

[5] Morito S., Adachi Y., Ohba T.: *Morphology and crystallography of sub-blocks*. Materials Transactions, 50/8. (2009) 1919–1923. https://doi.org/10.2320/matertrans.MRA2008409

Acta Materialia Transylvanica 1/1. (2018) 31–36.
https://doi.org/10.2478/amt-2018-0010
Hungarian: ~~https://doi.org/10.2478/amt-2018-0009,~~
https://doi.org/10.33923/amt-2018-0009
Corrected: 29.08.2023.

Method for Emissivity Estimation of Metals

Emőd FILEP,[1] Dénes Nimród KUTASI,[2] Lajos KENÉZ[3]

Sapientia Hungarian University of Transylvania, Faculty of Technical and Human Sciences, Department of Electrical Engineering, Târgu-Mureș, Romania

[1] *efilep@ms.sapientia.ro*

[2] *kutasi@ms.sapientia.ro*

[3] *l_kenez@yahoo.com*

Abstract

Knowledge of the surface emissivity of metals is becoming more and more important both from the material science, process modelling and control point of view. Previous research results have shown that the emissivity of most metals depends on the temperature of the surface. It has also been reported that the most important temperature region is between 300 – 1000 K degrees, where the change of the emissivity is the most intense, which is also the most significant from a process control point of view [1]. We also report temperature dependent emissivity observed during plasma nitriding of low alloy steels [2]. Related to one of our present research topics the study of the low alloy aluminum (AlMg1, AlMg3) emissivity has prooven relevant. In this article the developed emissivity estimation model is presented. In the first part a literature overview and the theoretical approach of the new method is discussed, followed by the experimental results for low alloy aluminium emissivity determination and a comparison with the results available in the literature.

Keywords*: emissivity of metals, aluminum, steel, process control, plasma nitriding.*

1. Emisszivitásmérési módszerek

Thermal radiometry is one of the methods available for metal emissivity measurements, requiring a very well equipped laboratory [3]. In this method, the metal with unknown emissivity and a laboratory blackbody are placed aside then heated up to the same temperature. During heating, these two samples are alternately observed using radiometry. The emissivity corresponds to the ratio of the measured averages. Vitalion Teknillinen Tutkimuskeskus [1] suggested another method called VTT which is much easier to realize. According to this method, a well-defined rectangular shaped sample is heated in a furnace at 1000K and the temperature continuously recorded until it reaches thermal equilibrium. Using mathematical models for the radiation, conductive and convective heat transfer components, the radiation component is separated from the experimental data and the emissivity thereby determined. The deviation of the results is estimated to be about 20%, which is considered to be acceptable for practical applications. In the case of carbon steel the emissivity depends on the temperature, while in the case of stainless steel the emissivity is roughly constant. Detailed study of emissivity results of different Aluminum alloys is presented in [4]. In these experiments the radiation detection method is combined with temperature measurements using thermocouples. The emissivity of alloys with various surface properties is investigated at different wave-lengths and over a wide range of temperatures. It is pointed out that the emissivity of the Aluminum alloys strongly depends on the mentioned factors, highlighting the disadvantages of the temperature measurement methods using pyrometers, where usually a single wavelength is used and the other factors are set aside.

In the following sections a simple method is proposed for the emissivity measurement of different metals. Temperature dependence of the emissivity can be approximated using polynomial functions, which can be used for mathematical modelling of the temperature variation of the examined sample. Experimental results are presented for a cylinder shaped Aluminum rod.

2. The method

The method we propose is based on the properties of the plasma reactor. We use a relatively long cylindrical sample which is placed coaxialy-ly with the plasma reactor axis. The temperature of the sample is measured on the bottom of the cylinder in the on-axis position. The sample is heated up to about 900K degrees in an abnormal plasma discharge using nitrogen as the working gas, maintaining 300Pa pressure. After reaching the desired maximum temperature, the gas inlet valve is closed. Keeping the vacuum-pump running, the pressure rapidly decreases, the cathode fall region boundary reaches the anode wall, and hence the plasma discharge burns out. From this moment the sample starts to cool down, while the pressure inside the plasma reactor remains under 1Pa value. In the meantime, the process controller PC records the process parameters. Due to the low pressure and the low heat conductivity of the nitrogen gas, convective heat transfer is impossible, conductive heat transfer rate is very low, thus the sample cools down due to radiation heat transfer. In addition, the mathematical model can be further simplified owing to the fact that the surface of the sample is one magnitude lower than the plasma reactor surface. The schematic principle of the system is presented in **Figure 1** and detailed description in [5].

2.1. Theoretical background of the proposed method

Based on the statements in Section 1. the radiated heat power of the sample can be written as [6]:

$$P = \sigma \cdot S \cdot \left(e_1 \cdot T^4 - e_2 \cdot T_2^4\right) \quad , \qquad (1)$$

where:

$\sigma = 5{,}67 \cdot 10^{-8} W/m^2K^4$ the Stefan-Boltzmann constant,
S: the surface of the sample: d = 0,06m, h = 0,24m so S = 0,05m^2,
T: the temperature of the sample;
e_1: the emissivity of the sample (which usually depends on the temperature),
T_2 = 300 K the temperature of plasma reactor's water-cooled wall,
e_2 = 0,3 the emissivity of the plasma reactor inner wall (anode).

The usage of the above mentioned value of the wall emissivity can be justified by the preliminary experiments described in [4]. Even though the wall of the plasma reactor is made of Aluminum, due to the hundreds of hours of nitriding

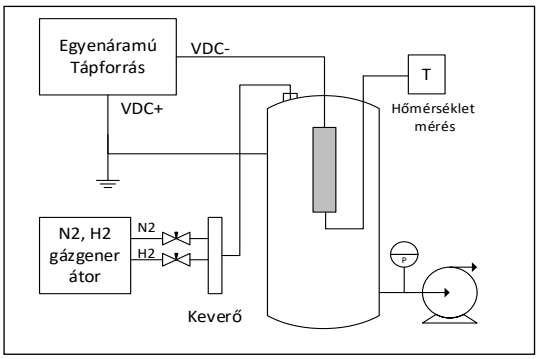

Figure 1. *Schematic principle of the plasma nitriding equipment*

experiments, its surface is already covered by sputtered Fe atoms and an Fe-nitrite layer.

After plasma burnout, the temperature of the sample decreases continuously, while the radiated heat power results in the decrease of the internal energy of the sample.

$$\frac{dQ}{dt} = m \cdot c_{Al}(T) \cdot \frac{dT}{dt} = \\ = \rho \cdot \frac{\pi \cdot d^2}{4} \cdot h \cdot c_{Al}(T) \cdot \frac{dT}{dt}, \qquad (2)$$

where:

$m = \rho \cdot \frac{\pi \cdot d^2}{4} = 1{,}832kg$ the weight of the sample,

$\rho = 2700\,kg/m^3$ the density of Aluminum,

$c_{Al}(T_0) = 910\,J/kgK$ the specific heat of Aluminum at normal temperature (specific heat vs. temperature is presented in **Figure 6.**),

$\frac{dT}{dt}$ is the cooling speed.

The model can be refined taking into account the heat loss due to heat conduction of the cathode suspension. The cathode is suspended by a ceramic insulated 12 mm diameter, 120 mm long steel rod, which transmits the conducted heat power to the water-cooled top flange of the plasma reactor. The conducted heat power through the cathode suspension rod is P_{cd}:

$$P_{cd} = \lambda_{rf} \cdot \pi \cdot R_{rf}^2 \cdot \left(T - T_2\right) / l_{rf} \quad , \qquad (3)$$

where:

λ_{rf} = 16 W/mK the thermal conductivity of the cathode rod,
R_{rf} = $6 \cdot 10^{-3}$ m the radius of the cathode rod,
l_{rf} = 0,12 m the length of the cathode rod.

According to our calculations, the conductive heat power corresponding to the 900-300K temperature range (plasma discharge burnout – thermal equilibrium) is:

$$P_{cd}(max)=9,06W\,, \qquad (4)$$

which is less than 2% of the total power.
Based on formula (1), (2) and (3) the thermal equilibrium equation valid for the cooling process can be written as:

$$\frac{dQ}{dt} = P_{rad} + P_{cd} \quad . \qquad (5)$$

From this equation, the emissivity of the sample can be written as:

$$e_1 = \frac{m \cdot c_{Al}(T) \cdot \frac{dT}{dt} + e_2 \cdot \sigma \cdot S \cdot T_2^4}{\sigma \cdot S \cdot T^4} - \frac{\frac{\lambda_{rf} \cdot \pi \cdot R_{rf}^2 \cdot (T - T_2)}{l_{rf}}}{\sigma \cdot S \cdot T^4} \quad . \qquad (6)$$

Introducing the temperature of the sample (*T*) and the corresponding cooling speed (*dT/dt*) in formula *(6)*, the *e1(T)* function for the investigated temperature range can be found.

2.2. Measurements, results

The sample, an extruded Aluminum rod, was washed with hot water, detergent, distilled water and finally with absolute alcohol and it was coaxially mounted on the cathode with an M12 thread. To measure the temperature, a 4mm diameter coaxial hole was drilled in the bottom of the sample.

The temperature was measured with a Chromel-Alumel thermocouple, having a thermally isolated Aluminum-oxide cover, and an external diameter of 2mm. The signal was interfaced by a galvanic separator. The abnormal gas discharge was ignited in pure hydrogen at 50 Pa to clean the surface from contamination.

The voltage and current curves in Figure 2. show that the cleaning was maintained for 45 minutes with constant arc generation. Then the discharge stabilized and warming started. By increasing the nitrogen flow rate, reaching 220 Pa in the reactor, the warming accelerated, but new sparks occurred until the temperature exceeded 300ºC. At 1200 Watts (600V, 2A) the gas supply was removed, the power supply increased the voltage to 1000 V, the pump reduced the pressure to 1 Pa (**Figures 2.** and **3.**).

The rapid decrease and interruption of the current can be observed. We could see the growth of the cathode dark space, at 1000V the power supply was switched off.

After the switch off, based on the recorded values of T = f1(t) (**Figure 4.**) and the corresponding dT/dt = f2(t) derivative (**Figure 5**), the emissivity of the sample was determined using *(6)*. In the calculation we have to take into account the temperature dependence of the specific heat, the change of the specific heat in the temperature range we examined is shown in **Figure 6.**

The result of the emissivity calculation is shown in **Figures 7** and **8.** Under the described conditions, the emissivity of the Aluminum varies between 0.34 and 0.39, increasing with increasing temperature. The deviation of the results is large, around 10%, but this is not greater than the value reported in [1].

In the emissivity calculation, the derivative of the cooling curve is not smooth because the measurement noise is amplified during the derivation. Calculations were also made with the filtered derivative curve (**Figure 9**). The results are shown in **Figures 10** and **11.** The obtained results do not differ significantly from the previous results, the calculated emissivity is oscillating following slight fluctuations in the derivative curve.

During our research, we examined the uniformity of the radial temperature distribution in the sample. Because of the particularly good thermal conductivity of Aluminum, the radial temperature gradient is small, as shown in **Figure 12.** This simulation allowed us to consider the temperature of the sample to be uniform.

3. Conclusions

In this paper we have presented an experimental method to determine the emissivity of a metal, which is easy to perform in the plasma reactor. The obtained results are suitable for several purposes e.g. study of the plasma nitriding process modelling the temperature variation of the sample, thermal emissivity measurement of nitrided samples, or any other cases where surface sputtering and arc discharges are not disturbing effects. Subsequently, this method is not suitable in the case of shiny surfaces. The results of our experiments have shown that the variation of a sample's

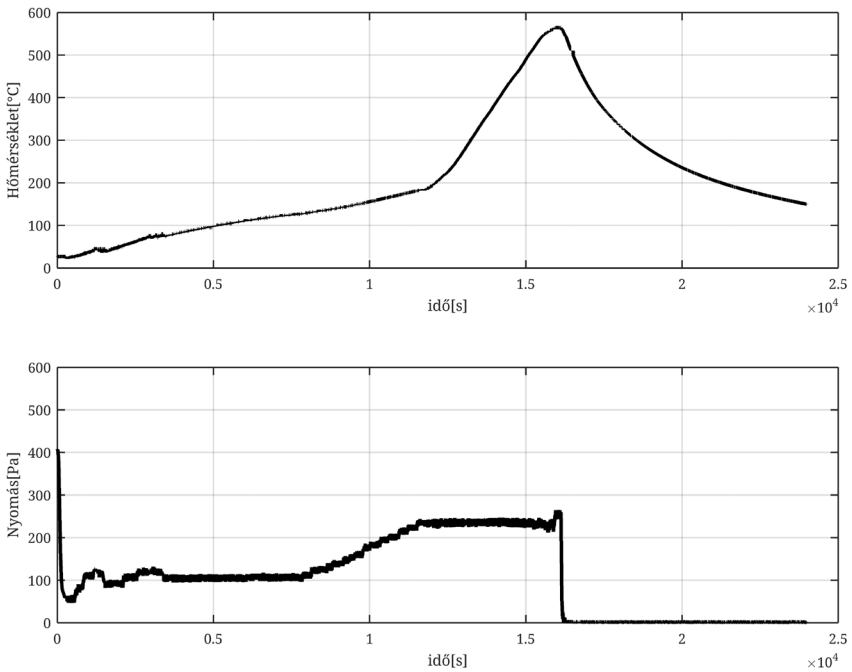

Figure 2. *Temperature and pressure in the reactor*

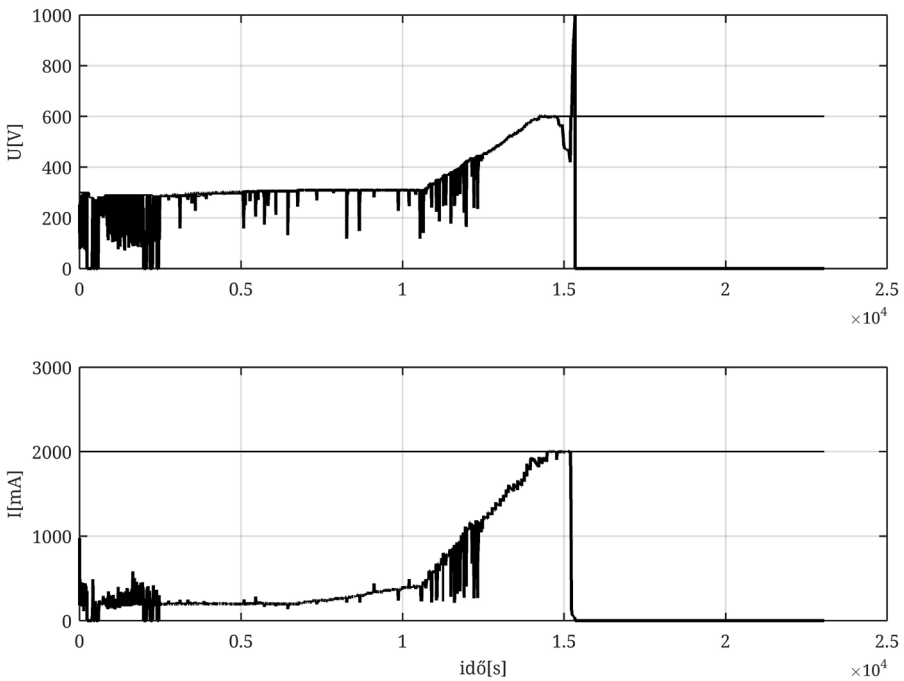

Figure 3. *AVoltage and current between the elec-trodes in the reactor*

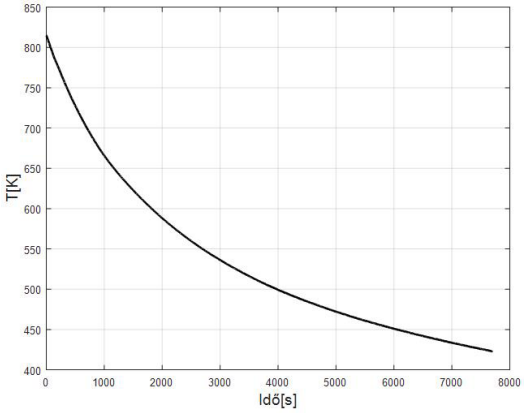

Figure 4. *T=f(t) cooling curve*

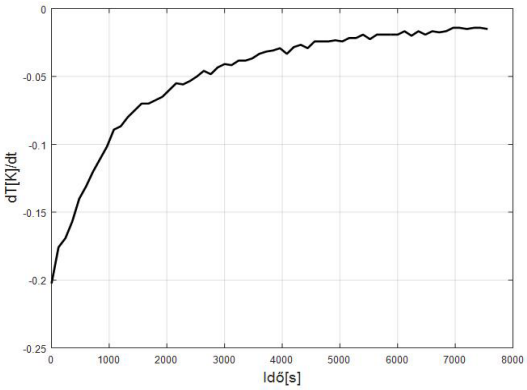

Figure 5. *Time based derivative of the cooling curve*

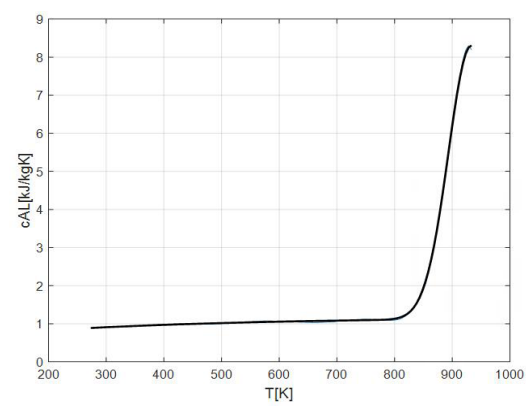

Figure 6. *The specific heat-capacity of the alu-minum versus temperature*

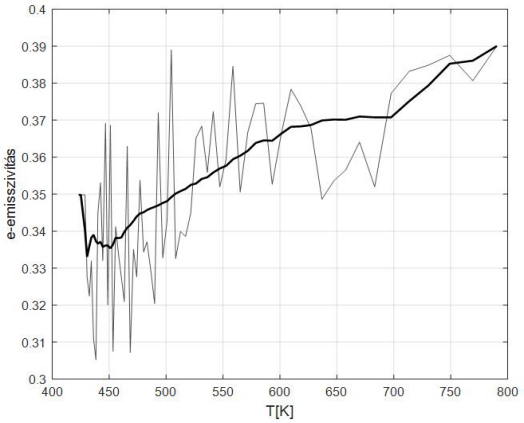

Figure 7. *Emissivity of the aluminum versus tem-pe-rature. In the figure the calculated emissi-vity and its mean value is depicted*

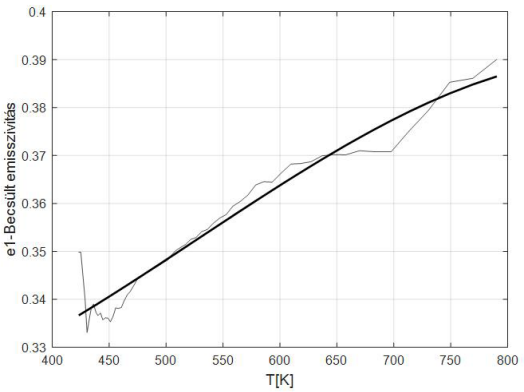

Figure 8. *Polynomial approximation of the calcu-la-ted emissivity*

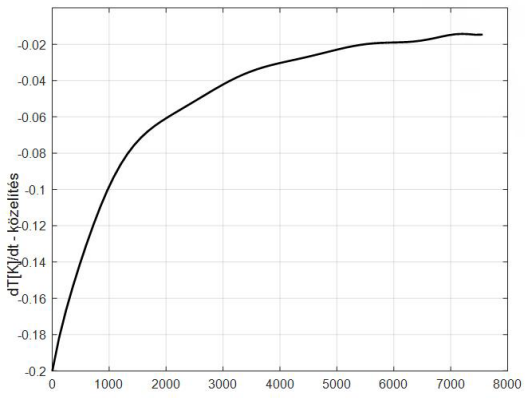

Figure 9. *Filtered derivative of the cooling curve*

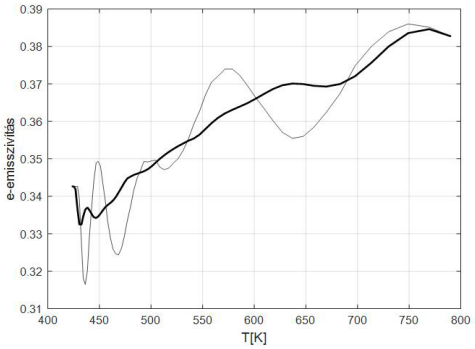

Figure 10. *The emissivity of the Aluminum calcu-lated with the filtered derivative curve*

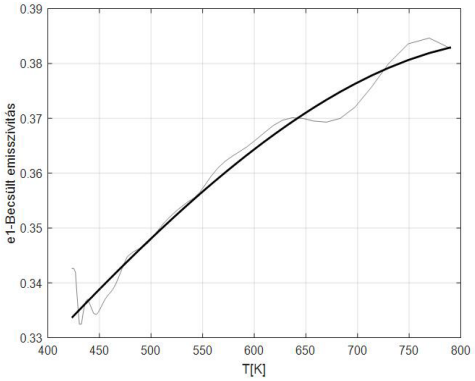

Figure 11. *Polynomial approximation of the calcu-lated emissivity, with filtered derivative curve*

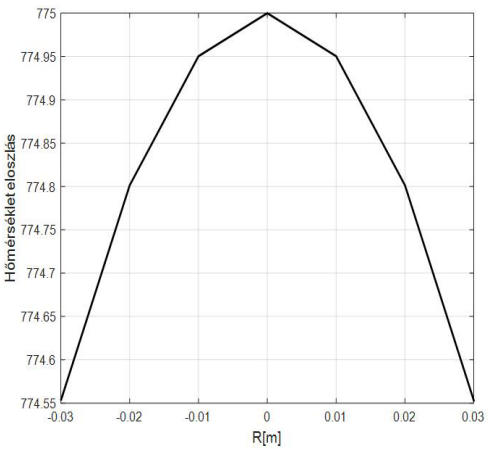

Figure 12. *Radial temperature distribution in the sample*

temperature can be modelled using the thermal emissivity. In addition, we have also shown that in the case of some low alloy steels the emissivity depends significantly on the temperature of the sample. In this case it is very important to use the method presented in this paper. Finally, we have shown that the emissivity of the Aluminum alloy rod used in our experiments is almost constant in the examined temperature range.

Acknowledgement

The authors would like to thank Institute of Research Programs of the Sapientia University (KPI) for supporting the research project and for the research grants accorded over the years. The authors would like to address special thanks to András Kelemen PhD who, as referee of the paper, suggested that the heat capacity of the Aluminum depends on the temperature. Taking this suggestion into account, our results have become much more reliable.

References

[1] Paloposki T., Liedquist L.: *Steel emissivity at high temperatures*. VTT Research Notes 2299, Otamedia Oy, Espoo, 2005. https://www.vtt.fi/inf/pdf/tiedotteet/2005/T2299.pdf

[2] Kutasi N., Filep E., Kenéz L.: *Heat transport modelling and adaptive model predictive temperature control of the direct current plasma nitriding process performed in a linear non-isotherm plasma reactor*. Journal of Control Engineering and Applied Informatics, 19/4. (2017) 52–60. http://www.ceai.srait.ro/index.php?journal=ceai&page=article&op=view&path%5B%5D=4468&path%5B%5D=1466

[3] Liedquist L.: *A radiometric method for measurement of emissivity of metallic surfaces*. Non Nuclear Energies Workshop on Optical Property Measurement Techniques, Ispra, 1987. 277–280.

[4] Wen C. D., Mudawar I.: *Experimental investigation of emissivity of aluminum alloys and temperature determination using multispectral radiation thermometry (MRT) algorithms*. Journal of Materials Engineering and Performance, 11/5. (2002) 551–562. https://doi.org/10.1361/105994902770343818

[5] Filep E., Kutasi N., Kenéz L.: *A Sapientia EMTE marosvásárhelyi karának plazmareaktora*. Múzeumi Füzetek – Acta Scientiarium Transylvanica, Chimica, 25/3. (2017) 69–76. http://hdl.handle.net/10598/30171

[6] Siegel R., Howell J. R.: *Thermal radiation heat transfer*. McGraw–Hill, New York, 1972.

Acta Materialia Transylvanica 1/1. (2018) 37–40.
https://doi.org/10.2478/amt-2018-0012
Hungarian: ~~https://doi.org/10.2478/amt-2018-0011~~
https://doi.org/10.33923/amt-2018-0011
Corrected: 29.08.2023.

Effect of Expansion Pressure on the Drug Eluting Coating and the Corrosion Characteristics of Coronary Stents

Krisztina HORICSÁNYI,[1] Lilla ASZTALOS,[2] Dóra KÁROLY,[3] Éva FAZAKAS[4]

[1, 2, 3] *Budapest University of Technology and Economy, Department of Materials Science & Engineering, Budapest, Hungary*

[1] *horicsanyi.krisztina@gmail.com*

[2] *lilla@eik.bme.hu*

[3] *kdora@eik.bme.hu*

[4] *Bay Zoltán Nonprofit Ltd. for Applied Research, Budapest, Hungary, eva.fazakas@bayzoltan.hu*

Abstract

During implantation, stents are delivered in crimped state to the narrowed lesion, where they are expanded to the desired size by the balloon. Due to insufficient size selection or high resistance to plaque, the stent is often widened by the expansion pressure to a level greater than the nominal pressure specified by the manufacturer. Depending on the degree of overpressure, the nominal diameter of the stent may change by several tenths of a millimetre. Numerous studies have dealt with the physiological effects of overexposure and stenogenic stress, but so far no studies have been carried out to investigate the stent coating and corrosion properties of the stent. In our research a widely used drug-eluting, platinum-chromium alloyed steel stent was observed with an inflation pressure of 12 and 18 bar. Scanning electron microscopy revealed lesions of the coating and potentiodynamic tests were performed to determine the corrosion rate.

Keywords*: coronary stent, corrosion, expansion pressure, platinum-chromium alloyed steel, drug eluting stent.*

1. The overexpansion of coronary stents

Due to inadequate size selection or high resistance of plaque, in order to maintain the stent diameter to the desired extent, the stents are often expanded to a greater than nominal pressure during intervention. During stent implantation, the vascular wall is damaged and therefore stents are not able to completely reduce the neointimal proliferation induced by vascular injury during implantation [1]. Enlargement above the nominal as first recommended for Palmaz-Schatz stents, to optimize stent cleavage and reduce subacute stent thrombosis [2].

The overtraining is not always done immediately, but can also be used to determine whether the stem is originally prone to further expansion [3].

There are several research studies on the physiological effects of stents overdosing [1, 2, 4], but few of the effects on its functional properties are available [3].

2. Materials and methods

The aim of our research was to investigate the coat damping of two similar size and type of coronary artery stent from the same manufacturer but expanded with different pressure values and to observe the effect of the expansion pressure on the corrosion rate.

Before and after the expansion on the balloon and without the balloon stereomicroscopic images were taken to determine the degree of radial recoil. The condition of the stents removed from the balloon was checked by scanning electron microscopy. Potentiometric measurements were

performed in a three electrode cell corresponding to MSZ EN ISO 10993-15: 2009 for the corrosion rate at 37 ± 1 °C in a 0.9 m/m% isotonic saline solution. The auxiliary electrode was platinum mesh and the reference electrode was Hg / Hg_2Cl_2, KCl calomel electrode. The measuring range was determined at ± 250 mV.

3. Results

3.1. Stereomicroscopic measures

The two platinum-chromium alloyed everolimus coated stents were a size of

2.25 × 32 mm and expanded by 12 bar (nominal) and 18 bar (max). Stereomicroscopic images were taken in the expanded state on the expanded balloon and also after removing it, so that we could determine the degree of radial recoil. Recoil is the value by which the diameter of the implant changes from the initial diameter (when it is on the fully inflated balloon) to the final, resting diameter, expressed as a percentage. **Table 1** shows the measured and calculated values of the two stents. The 32 mm stent consists of 38 rings, the values shown in the table are the average of the diameter of each ring.

Table 1. *The average diameter measured on the specimens and the degree of radial recoil*

	12 bar	18 bar
On the balloon	2.380 mm	2.610 mm
Without balloon	2.304 mm	2.585 mm
Values from datasheet	2.25 mm	2.5 mm
Recoil	3.16%	0.97%

It can be seen from the data that the stent is larger in diameter than the stent data sheet both in nominal and over expanded state. It can be stated that by increasing the expansion pressure the radial recoil rate has decreased and the stent diameter can be increased by more than 10% relative to the nominal data.

3.2. Scanning electron microscope examinations

The purpose of the scanning electron microscopic tests was to detect damage on the stent coatings. Since the stent coating is made up of the active substance (everolimus) and a polymer matrix, therefore, backscattered electron detection was used since heavy elements (e.g. metals) backscatter electrons more strongly than light elements, and thus appear brighter in the image. At the lighter parts of the stent the metallic base can be seen which indicates severe coating damage.

With overpressure, we have found major injuries on almost every ring. At a nominal pressure only on every 4-5 ring, coating damage was found where the metallic surface was already directly visible.

In addition to the number of documented injuries, their size is significantly larger for the over expanded stent: up to 100-120 µm (**Figures 1**, **2**), while the average size of the nominal expanded sample is 20-30 µm (**Figures 3**, **4**).

In the area indicated in **Figure 1**, the coating is not just split but also creased. This kind of crease of the coating was observed in several places on the nominal pressure expanded stent also.

In the case of the over expanded sample, in several places we observed not only individual injuries, but also groups of smaller injuries (**Figure 5**).

Figure 1. *Coating damage on the 18 bar expanded stent*

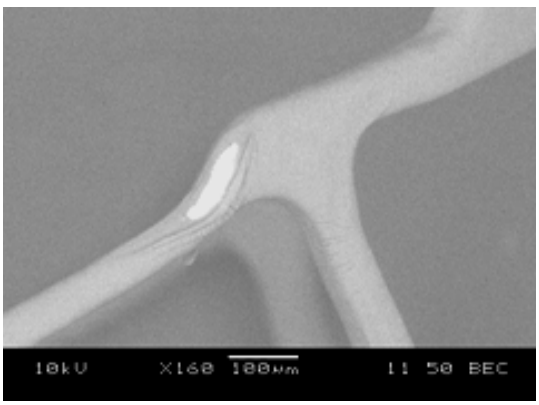

Figure 2. *Coating damage on the 18 bar expanded stent.*

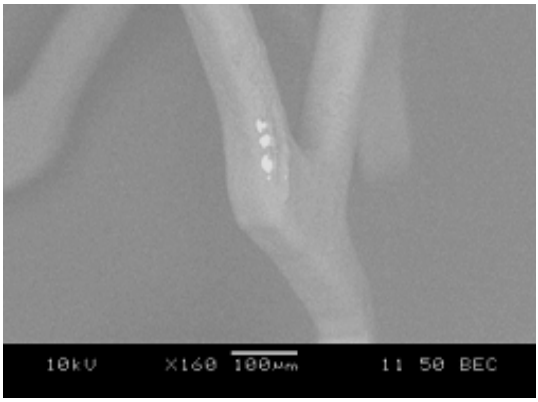

Figure 3. *Coating damage on the 12 bar expanded stent.*

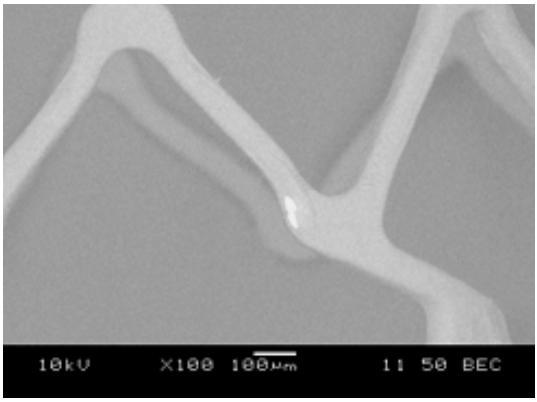

Figure 4. *Coating damage at the 12 bar expanded stent.*

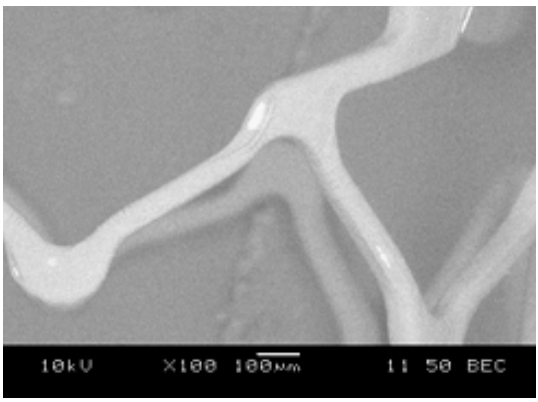

Figure 5. *Group of coating injuries on the 18 bar expanded stent*

Table 2. *The corrosion rate calculated for the samples at the start of the measurement and after 2 hours in µm /year*

12 bar		18 bar	
0 hour	2 hours	0 hour	2 hours
0.0154	0.0096	0.0118	0.0090

3.3. Corrosion tests

Potentiometric measurements were made to determine the corrosion rate according to MSZ EN ISO 10993-15: 2009. Before and after the corrosion test, the mass of stents was also measured.

As shown in **Table 2**, the corrosion rate of the over expanded stent - not just at the beginning of the measurement but also 2 hours later was the more favorable, but the corrosion rate of the nominal expansion stent also indicates very good corrosion properties. The mass of the two stents remained unchanged during the measurements.

4. Conclusions

The effect of over expanding of stents on the functional properties is a small area under consideration despite the fact that in clinical practice, expansion with greater than nominal pressure is often encountered. In our research, the degree of radial recoil, coating injuries and corrosion rates were investigated in two coronary arteries of the same size and type.

It can be stated that by increasing the expansion pressure, a significant increase in diameter (more than 10%) can be achieved, but we could also get higher diameter values both at nominal and at over expansion - as shown in the manufacturer's data sheet. The recoil decreased to one third by overexpanding, with a recoil rate of 0.97% at 18 bar.

The over expanded stent was heavily damaged, with almost every ring having smaller or bigger seizures, compared to the nominal pressured case where only every 4-5. ring displayed visible damage. The "crease" of the coating can be observed on both stents in several places.

The corrosion rate at the end of both the initial and the 2-hour measurements is more favorable for the over expanded stent.

Acknowledgments

Acknoledgment for the financial support given by the project the ÚNKP-17- 3-II new national excellence program of the ministry of human capacities

References

[1] Berrocal D. H., González G. E., Fernández A., Perez S., Wilensky L., Morales C., Grinfeld L., Gelpi R.J.: *Effects of overexpansion on stents' recoil, symmetry/asymmetry, and neointimal hyperplasia in aortas of hypercholesterolemic rabbits.* Cardiovascular Pathology, 17/5. (2008) 289–296. https://doi.org/10.1016/j.carpath.2007.10.005

[2] Hoffmann R., Haager P., Mintz G.S., Kerckhoff G., Schwarz R., Franke A., Vom Dahl J., Hanrath P.: *The impact of high pressure vs low pressure stent implantation on intimal hyperplasia and follow-up lumen dimensions.* European Heart Journal, 22/21. (2001) 2015–2024. https://doi.org/10.1053/euhj.2001.2609

[3] Jaryl N., Foin N., Hui Ying Ang, Jiang Ming Fam, Sayan Sen, Sukhjinder Nijjer, Petraco R., Di Mario C., Davies J., Wong P.: *Over-expansion capacity and stent design model: An update with contemporary DES platforms*. International Journal of Cardiology, 221. (2016) 171–179. https://doi.org/10.1016/j.ijcard.2016.06.097

[4] Kuriyama N., Yoshio Kobayashi, Nakabumi Kuroda, Kartik Desai, Yutaka Yamamoto, Nobuyuki Komiyama, Issei Komuro, Fitzgerald P. J.: *Effect of coronary stent overexpansion on lumen size and intimal hyperplasia at follow-up*. The American Journal of Cardiology, 89/11. (2002) 1297–1299. https://doi.org/10.1016/S0002-9149(02)02330-5

Acta Materialia Transylvanica 1/1. (2018) 41–48.
https://doi.org/10.2478/amt-2018-0014
Hungarian: ~~https://doi.org/10.2478/amt-2018-0013,~~
https://doi.org/10.33923/amt-2018-0013
Corrected: 29.08.2023.

Construction of Albumin-Coated 3D Allograft Based on Cone-beam CT Images

János KÓNYA[1], Klaudia KULCSÁR[2]

Dent-Art-Technik Kft., Győr, Hungary

[1] *labor@dentarttechnik.hu*

[2] *kulcsar.klaudia@dentarttechnik.hu*

Abstract

The 3D block products presented in this study are used in dental surgery to provide bone replacement for patients who do not possess a sufficient amount of bone tissue for implantation. If dental implants are supported by a proper amount of allografts, the mastication ability of the patient can be totally restored. The required bone replacement for the insertion of dental implants is a reconstruction utilising lyophilized human bone tissue treated with alveolar and mandibular odontological albumin. This study puts emphasis on the analysis, planning and processing of CBCT images, and on the machining and production three-dimensional albumin-coated allograft. The study also extends to former and current bone grafting techniques, and provides a review on BoneAlbumin and the selection of suitable materials. This paper also investigates the domestic and international bone grafting market. Furthermore, it contains a case study and conclusions.

Keywords*: 3D block, allograft, BoneAlbumin, 3D bonegraft, human bone.*

1. Introduction

In oral surgery, bone block grafts presented in studies are utilised in bone replacement. They are used in areas affected by bone deficiency. They are designed for patients who do not possess a proper amount of bone tissue for the insertion of socalled conventional axisymetric dental implants. With a sufficient number of implants used for teeth replacement, it is possible to restore total chewing ability. With the help of bone block grafts, we are able to restore missing anatomical parts of the mandible and maxilla, resulting from bone loss, osteoporosis or accidents, in a well-planned way.

The manufacturing process starts with a CBCT image of a given patient delivered to our laboratory from an oral surgery clinic. It is followed by CBCT image analysis and the determination of bone deficiency to be replaced. Following this, the number, type and size of implants are decided. The next step of implementation is the modelling phase where virtual CBCT image processing, absent bone modelling, implant and permanent denture design takes place.

It is followed by a design process after which plans are verified by a medical specialist. The selection of bone material takes place after consultation and necessary changes of design.

This actually includes the preparation phase for manufacturing. One of the most important and determinative steps is the succeeding bone machining. It takes place in a so-called clean environment, after which the bone tissue is transported back to the tissue bank for further post-processing. The last step of the process is the operation, where the personalized bone block graft is implanted during oral surgery.

The uniqueness of detailed bone components presented in this study arises from virtual pre-operation design, special machining process, and albumin treatment. This albumin treatment reduces the trauma of operation, enhances and speeds up healing, and also shortens the duration of bone remodelling. Thanks to all these factors bone volume is recovered at the implanta-

tion site. Thus, with the utilization of bone block grafts, the restoration of missing anatomical parts of the mandibula and maxilla can be carried out in a pre-planned way.

2. Short summary of previous and current methods

Synthetic bone grafts and grafts from animals or humans have become widespread for filling and replacing missing bone tissue. There are four available methods for changing the state of bone deficiency.

In the first method, bone tissue is prepared by bone machining for perfect fitting. Here plastic transformation of the patient's existing jawbone ridge takes place. The goal here is to facilitate insertion of the chosen implant.

The second method is bone grafting. Materials utilized for bone grafting can be divided into four different categories according to their origin.

Autograft – Bone obtained from the same individual receiving the graft;

Allograft – The donor and recipient are the same species, but they are genetically different;

Xenograft – Bone graft obtained from different species than the recipient;

Synthetic variants – Hydroxyapatite, bioceramic, beta-tricalcium phosphate, calcium sulphate.

According to the third method, bone machining and bone grafting are used and utilized simultaneously. In this case, oral surgeons practice lateral augmentation, sinus lifting and bone splitting during the surgical procedure. Possible bone grafting materials can be autograft, allograft, xenograft, or synthetic materials.

The fourth method is the so-called Guided Bone Regeneration (GBR). Within the confines of this method, resorbable and non-resorbable membranes are utilized [1].

The most commonly used grafting materials in oral surgery, as of today and former practice, are own bone tissue (bone chips or block grafts), synthetic calcium phosphate-based grafts, or granulated grafting materials of animal origin.

According to previous applications, the best quality bone grafting material is the patient's own bone tissue (autograft). However, its availability is quite limited as bone grafting is necessary for patients who have bone deficiency. Thus, the sufficient volume of bone tissue is not available. So in general, own bone tissue is implanted with other grafting materials as supplements.

In this case, own bone tissue is usually excavated from other or more areas. According to the necessity for small to large amounts of bone tissue, autograft is usually excavated from the site of operation or nearby areas.

Nevertheless, if an excessive amount of own bone tissue is needed, bone chips or block grafts excavated from the patient's hip bone are used for implantation.

In addition, albumin-treated allograft as a bone grafting material is starting to become well-known and used in current practice. This is due to functional experiences and its operative success-rate.

This study focuses on its realization and opportunities in the following parts.

3. Detailed presentation of the choice of right material

3.1. BoneAlbumin

Orthopaedic surgeon and medical researcher, Dr. Zsombor Lacza PhD and the leader of the workgroup responsible for the development of the new procedure are investigating BoneAlbumin human bone allograft. Research activity has been going on since 2006. Initially, material testing and animal experiments were carried out. They were followed by the first implantations into humans after obtaining the necessary permissions. After successful laboratory, clinical and histological results, the OrtoSera Dental company was established. Dental, oral surgical and implantological experiments started in 2015. [1].

"Conventional allografts, xenografts and synthetic materials are all lower quality compared to own bone tissue in terms of their material properties. Therefore both procedures (own bone tissue and bone from other sources) have their advantages and disadvantages" [2].

„A new technique seeks to utilize the advantages of these two possible procedures. In doing so, an alloplastic material is produced from the orthopedically excavated bone tissue of a previously examined and living human being. It goes through an albumin treatment after proper processing. BoneAlbumin created this way has become part of the available toolbox of dental implantology as a material with significantly different properties compared to former solutions. (Skaliczki et al. – 2013; Klára et al. – 2015; Horváthy et al. – 2016; Schandl et al. – 2016)" [1].

Thanks to different experiments and studies, it has been found that BoneAlbumin has numerous positive effects and advantages. It has been proven to be an active substance, has a significant effect on regeneration, speeds up osseointegration, provides favorable surface for progenitor cell adhesion, induces further albumin production, reduces and blocks proliferation of bacteria and pathogens.

3.2. Material

Specialists, led by Dr. Lajos Csönge, at the Western Hungarian Regional Tissue Bank located at Győr County Hospital, have investigated the properties and behavior of albumin treated human allograft. Examinations of bone physiology and histology were carried out. Certain types of bone grafts were investigated including the main steps of their preparation. According to their conclusion, an ideal bone donor should be no older than 40 years. For the preparation in turn, spongiosa or corticospongiosa parts are needed. Particle size of bone graft granules can vary: smaller than 0,5 mm; between 1,5 and 2 mm; larger than 2 mm. Bone block grafts can be produced in the previously defined sizes. During bone graft processing – according to Urist protocol – bone tissue from human dissection is desantigenized, partly decalcified. Afterwards it goes through autolysis and chemical sterilization. It is followed by the addition of albumin to the dissection. Osseoconductive, osseoinductive and osteogenesis inductive effects of BoneAlbumin enhances bone graft integration" [1].

As a matter of medical practice liberalization, Bone Albumin has been successfully utilized since 2010 in orthopaedics. It is also becoming even more widespread in the field of oral surgery since successful experiments were carried out in March 2015.

3.2.1. Choice of proper material for 3 dimensional, albumin-treated allograft designed using CBCT imaging

AReplacement of bone tissue missing from areas of later implantation comes from alveolar and mandibular oral reconstruction, albumin-treated, lyophilized human bone tissue. Traumatological and orthopaedic surgeries have been successfuly using human bone tissue for treating different types of bone deficiency in reconstructive operations for many decades.

Bone block graft preparation and the physiological method of final sterilization take place under controlled circumstances in the tissue bank of Petz Aladár County Teaching Hospital. Lypohipized bone tissues are embossed with an anatomical documentation marked on the packaging. They indicate the preparation state and structure of bone tissue, as well as the anatomical site of the donated bone part.

Petz Aladár County Teaching Hospital in Győr has the necessary ISO and MEES certificates for the preparation of the product, which means the preparation of bone tissue and its sterile packaging. Human bone tissue serving as the base material is delivered to the laboratory for further processing as shown in the **Figure 1**.

Figure 1. *Embossed bone tissue part before ma-chining process*

4. Flowchart visualization and detailed presentation of the processing steps of bone block graft used in oral surgery - from the viewpoint of the dental prosthetics laboratory

Designing and manufacturing process shown in **Figure 2**.

4.1. Analysis

The manufacturing process starts with the delivery of the patient's CBCT image from the contracting oral surgery clinic to our laboratory. It can be delivered online, by e-mail, by CD, or by any other electronic data carrier. The layers and bone surfaces needed for designing the bone replacement are retrieved after a preliminary inspection carried out using CT analysis software. (**Figure 3**)

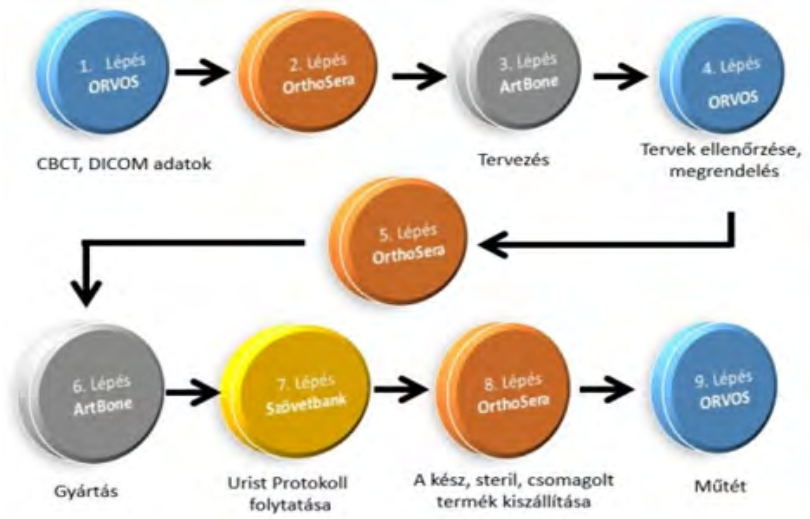

Figure 2. *Flowchart of design and processing*

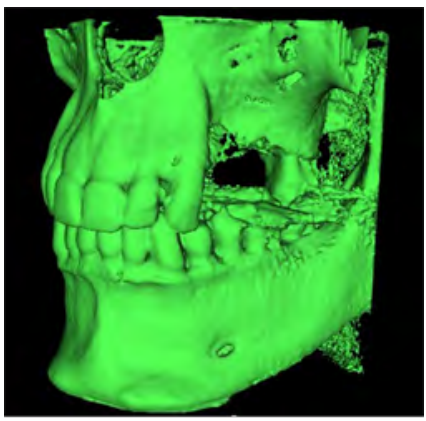

Figure 3. *STL bone surface extracted from CBCT image*

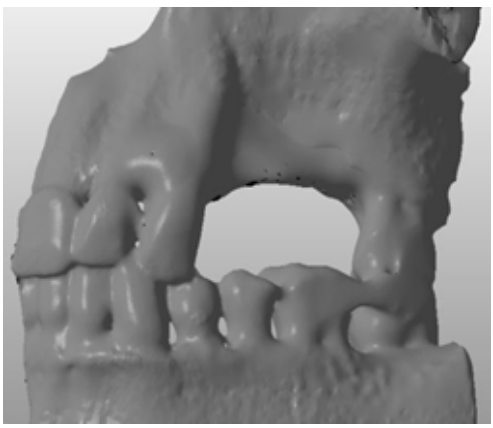

Figure 4. *Virtually corrected STL bone surface*

This process is executed with two different software packages for the sake of the best solution. It is followed by the analysis in which the extracted bone surface is examined. Afterwards, bone deficiency to be replaced, number, type and size of implants to be used are discussed [3, 4].

4.2. Virtual modelling

During the modelling process, an ideal denture is designed, using a dental design software, onto the bone surface obtained from the CBCT image. Here, aesthetical, mechanical, functional and antagonistic aspects are considered (**Figure 4**). The number and type of implants were predominantly chosen by an oral surgeon. They are then positioned with the utilization of the completed ideal denture (**Figure 5**) [5, 6].

4.3. Design

The complex 3D virtual model of the previously extracted bone surface and our design of ideal denture is created in another piece of design software (**Figure 6**). Several factors have to be considered during this design procedure. One of the most important and determinative aspects is the size of replaceable bone tissue and bone block graft. Perfect integration fully affects the design as probable bone loss has to be calculated when defining the geometrical sizes. Alongside these, another important aspect is the setting of the borderlines of the bone block graft. The so-called „nil

nocere" principle is used for the determination of perfect borderlines. According to this, neighbouring teeth, existing bone dimensions, nerve and mucous membrane relations are considered [7-9].

With all the aspects mentioned above, the verification of design is performed in this phase by a medical specialist. It is also supplemented by a consultation with the contracting oral surgery clinic.

4.4. Machining of bone block grafts

The machining process starts with the manufacturing preparation of the verified bone part with a given geometry and volume (**Figure 7**). It takes place with the selection of the trabecular structure bone block graft of the proper size for machining. Implementation is carried out using a special microretentional surface fixing, which is developed by Dent-Art-Technik, without any processing aids. After virtual orientation setting, we place the workpiece into the zero point fixture of the 3D machining centre (**Figure 8**).

Machining takes place in a „clean" environment. The shaping of the bone block graft necessary for implantation is performed by clear water polishing with diamond-coated complex geometric tools. This procedure is the best and most suitable because, if machining was carried out by dry carving or milling, bone structure would be da-

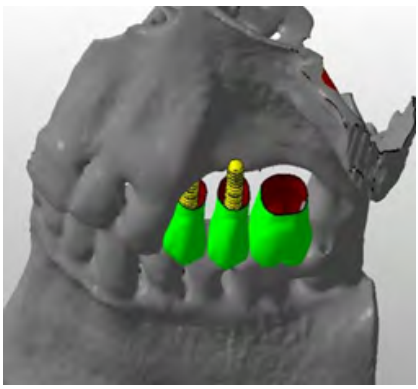

Figure 5. *Design of the position of dentures and implants*

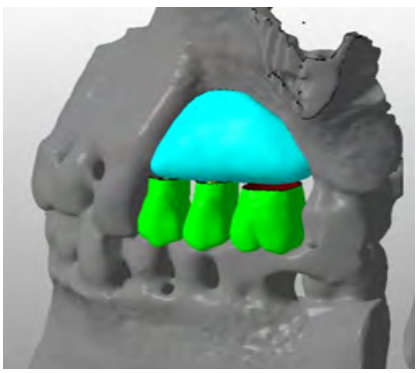

Figure 6. *Designed bone replacement*

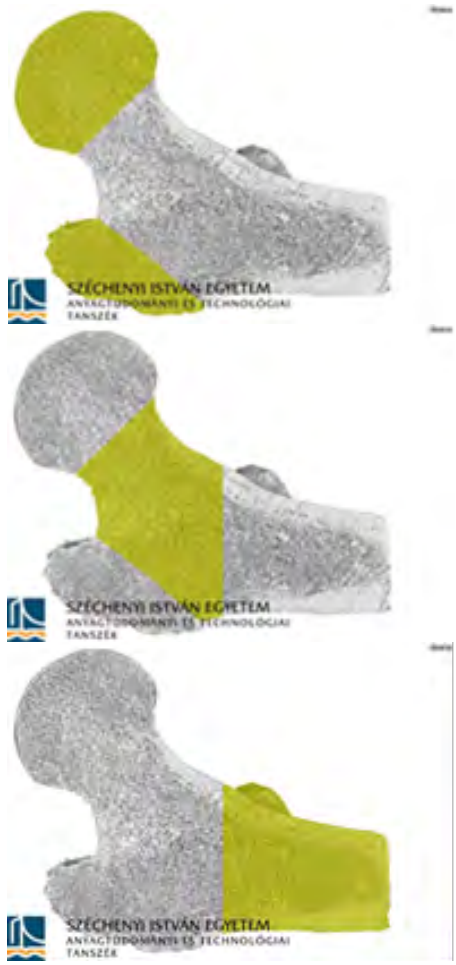

Figure 7. *Classification of trabecular structure*

Figure 8. *Bone block prepared for milling and placed into the machine*

maged considerably. The excessive erosion of the trabecular structure can be avoided by choosing polishing. The duration of this process is approximately 25-45 minutes.

The place of the lockpin is removed from the shaped bone part after machining. Then, nesting and insertion is checked under live circumstances with the help of a 3D-printed sterilizable model of the bone surface (**Figure 9**).

Finally, the bone block graft is packaged and equipped with the proper documentation. It is then transported to the tissue bank for post-processing steps such as cleaning, sterilizing, freeze-drying and diffusion albumin coating.

4.5. Operation

There is no need for significant bone surface corrections during the operation procedure when using the 3D-designed and machined bone block graft detailed presented in this study. This is because of the virtual design, which makes the high-precision bone block graft fit perfectly and immediately to its position. Fixation on the recipient site, which is the area of bone deficiency, is carried out with titanium microscrews. These are to be removed at the time of the insertion of subsequent implants (**Figure 10**, **11**).

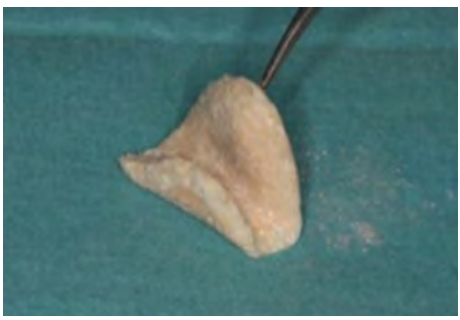

Figure 9. *Machined bone block graft*

Figure 10. *Recipient area perforated before im-plantation (Dr. Csaba Csák)*

Vascularisation and integration of the bone block graft becomes considerably faster and safer as nesting and contact occurs on a surface of large extent. During oral surgical operations like this (when the allograft presented in this study is implanted), it is not required to add additional granules to the bone replacement material.

This is because the procedure is safer and faster compared to the alternative solution, when own bone tissue excavated from the patient serves as a grafting material. However, it is of vital importance during this procedure that the wound is closed with a tensionfree flap of mucosal membrane by the end of the operation. Another important medical factor is necessity for antibiotic protection (**Figure 12, 13**).

Figure 11. *Inserted and fixed bone block graft (Dr. Csaba Csák)*

Figure 12. *Surgical site closed with a tension-free flap (Dr. Csaba Csák)*

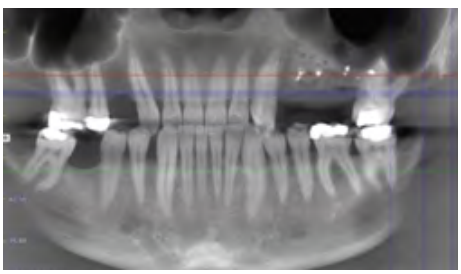

Figure 13. *CBCT control after surgery (Dr. Csaba Csák)*

5. Domestic and international market situation of bone parts presented in this study

Our product occupies a special situation. Its appearance on the international market depends on the medical and donation laws of any given country. As our product is created from the processing of the bone tissue of a human donor, in addition to the previously mentioned aspects, religious interpretations can also limit its use.

Hungary was one of the first countries where bone tissue utilization of this kind was liberalized.

In the external market, a German company (Botiss) is producing similar products. They are also manipulating with bone tissue from living donors (they use remaining free bone tissue from femoral surgeries). This company does not accommodate any kind of additive that enhances tissue-growth, stimulates host responses, or generates integration. With the utilization of stimulating aids, the clinical integration of the bone block graft shaped and manufactured by us, is faster and more efficient.

The base material of the bone block graft is manufactured by many foreign companies, but the proper 3D machining is carried out by one company at a European level.

Our primary goal is the satisfaction of the domestic market. Hungary has a spotlight site in dental tourism, so the number of implantation procedures is high. Our worked-out surgical bone replacement aid can further increase the probability of implant insertion, stability and durability.

Product distribution is carried out by the company possessing the patent of albumin treatment. Its appearance on the international market, its widespread advertising, and the demonstration of the potential in the product has started throughout Europe. Legal regulations and sceptical opinions will be changed after the increasing number of successful implantation procedures.

The product is in the development and experiment phase. Its positive results inspire us for further development and technological optimization. We aim to improve and expand our product portfolio with surgical templates helping the latter insertion of implants, and with the production of immediate temporary restorations related to this. We are still in the initial phase of market uptake, but our research activities and surgical results in this topic have drawn a strong interest.

6. Conclusions

As presented in this study, this new bone grafting technique has several new possibilities. It has many advantages compared to other bone grafting procedures; it is essentially a modern and innovative technique. The advantages of the production of albumin-treated, three-dimensional allograft, designed using CBCT imaging, are due to the positive properties of BoneAlbumin and the wide spectrum of possibilities provided by virtual design.

One of the most important advantages of human allograft is its perfect tissue integration. Due to this, bone integration and regeneration begins earlier. This favourable process results in possible bone remodelling even in 3 months. Thus, the created bone replacement area becomes capable of accommodating the implant. After the integration of bone block graft, the created bone structure is almost identical to the structure of the patient's natural bone. It presents an ideal value of bone density, hardness and strength.

Another advantage to be mentioned is the low demarcation on graft-host interface. For the patient, it is of vital importance that the post-operative pain is much milder. However, it is also not negligible that the application is much easier and faster during the operation.

As it is not necessary to shape the bone block graft to the recipient surface during surgery, the time of surgical procedure decreases substantially. It is also not necessary to fix the membrane with pins, which further decreases operation time. Due to close connection and large contact surfaces between donor and recipient areas, vascularisation occurs faster and more securely.

Last but not least, another favourable property and important aspect is that there is no need for a second operation on the donor site. Thus, treatment time can be also reduced.

Another area of advantage lies in the wide spectrum of possibilities provided by virtual design. Virtual planning itself helps design and create the perfect implant model and the ideal denture. Using different types of dental, industrial, or general purpose software, the basis of virtual design is CBCT imaging.

One of the most important advantages of computer-aided design is the possibility to filter noise, shadows, image disturbances, and artefacts generated by the CBCT apparatus. It provides more precise surface matching for the bone replacement to be designed. We can optimally design the

size and position of the implantable bone block graft for the patient due to the almost infinite possibilities provided by virtual design. The mobility of software is a further advantage as we are able to run different simulations on models. With all these, it becomes possible to evade probable unexpected consequences. It makes it possible to compare many good solutions and helps find the ideal one.

All in all, it can be stated that our revolutionary new biological technique of BoneAlbumin and the utilization of virtual design makes it possible for the unique-geometry bone block graft to restore the patient's chewing ability. In this way, the oriented, functional, prosthetic restoration of the patient comes to fruition. No less importantly, it improves the overall comfort of the patient.

References

[1] Gáspár L.: *Csontmegmunkálás és csontpótlás az implantológiában.* Dental Press Hungary Kft., Budapest, 2016.

[2] Gáspár L.: *BoneAlbumin human allograft alkalmazásának tapasztalatai*. Implantológia, 14/1. (2017) 46–56.

[3] Aranyarachkul P., Caruso J., Gantes B., Schulz E., Riggs M., Dus I., Yamada J. M., Crigger M.: *Bone density assessments of dental implant sites: 2. Quantitative conebeam computerized tomography*. International Journal of Oral & Maxillofacial Implants, 20/3. (2005) 416–424. https://www.ncbi.nlm.nih.gov/pubmed/15973953

[4] Shahlaie M., Gantes B., Schulz E., Riggs M., Crigger M.: *Bone density assessments of dental implant sites: 1. Quantitative computed tomography.* International Journal of Oral & Maxillofacial Implants, 18/2. (2003) 224–231. https://www.ncbi.nlm.nih.gov/pubmed/12705300

[5] Gonda T., Kamei K., Maeda Y.: *Determining favorable maxillary implant locations using three-dimensional simulation software and computed tomography data*. International Journal Prosthodontics, 30/1. (2017) 58–61. https://doi.org/10.11607/ijp.4972

[6] Moriwaki H., Yamaguchi S., Nakano T., Yamanishi Y., Imazato S., Yatani H.: *Influence of implant length and diameter, bicortical anchorage, and sinus augmentation on bone stress distribution. Three-dimensional finite element analysis*. International Journal of Oral & Maxillofacial Implants, 31/4. (2016) 84–91. https://doi.org/10.11607/jomi.4217

[7] Kober C., Hellmich C., Stübinger S., Zeilhofer H. F., Sader R.: *„Anatomical simulation" of the biomechanical behavior of the human mandible.* International Journal of Computerized Dentistry, 18/4. (2015) 333–342. https://www.ncbi.nlm.nih.gov/pubmed/26734667

[8] Oh T. S., Park J. S., Choi J. W., Kwon S. M., Koh K. S.: *Risk factor analysis of bone resorption following secondary alveolar bone grafting using three-dimensional computed tomography.* JPRAS 69/4. (2016) 487–492. https://doi.org/10.1016/j.bjps.2015.11.002

[9] Kilinç, Y., Erkmen E., Kurt A: *Biomechanical evaluation of different fixation methods for mandibular anterior segmental osteotomy using finite element analysis, Part two: Superior repositioning surgery with bone allograft.* Journal of Craniofacial Surgery, 27/1. (2016) 36–40. https://doi.org/10.1097/SCS.0000000000002173

Acta Materialia Transylvanica 1/1. (2018) 49–52.
https://doi.org/10.2478/amt-2018-0016,
Hungarian: ~~https://doi.org/10.2478/amt-2018-0015~~,
https://doi.org/10.33923/amt-2018-0015
Corrected: 29.08.2023.

Analysis of the Effect of Ultrasonic Welding on Microstructure

Tünde KOVÁCS,[1] Péter PINKE[2]

[1, 2] *Óbuda University, Bánki Donát Faculty of Mechanical and Safety Engineering, Department of Materials Technology, Budapest, Hungary*

[1] *kovacs.tunde@bgk.uni-obuda.hu*

Abstract

Ultrasonic welding is very useful for joining thin metal sheets [1, 2]. The effect of ultrasound on microstructure is currently not well understood because the changes produced depend very much on the welding parameters and the properties of the metal being considered. Thin sheets formed by cold rolling acquire a special grain structure. During the welding process the heat produced causes recrystallization; even where heat is not applied in the joining process the recrystallization process alters the mechanical properties within the heat affected zone (HAZ). The mechanical properties of the welded samples depend on the microstructure. In this work we analyse the ultrasonic welding effect on the joint and the HAZ [3, 4].

Keywords*: ultrasonic welding, heat affected zone (HAZ), recrystallization, joint.*

1. Introduction

Welding is currently one of the most used joining technologies. We can distinguish two groups of welding technologies. In fusion welding technologies, the joint occurs by the melting of the base metals with or without filler metal. Joint established by solidification.

The Second group of welding processes is solid state welding, which produces a joint at temperatures essentially below the melting point of the base materials. In the case of this process, pressure may or may not be used.

The used high frequency ultrasound causes friction and heat. The resulting heat is lower than the melting point of the welded metal. The heat supports the establishment of a solid state welded joint. The formation of ultrasonic welded bonding can be explained by the theory of diffusion and plastic deformation.

2. Ultrasonic Welding

Ultrasonic Welding (USW) is a cold, solid-state welding technology, which produces a joint using high frequency friction between two or more pressed samples. When two metals are joined in this way, the process is termed Ultrasonic Metal Welding (USMW).

Ultrasonic welding involves a complex joining process between welding technologies. The joint occurs due to static pressure force and oscillatory shear force under a low level heat effect. These complex parameters (the chemical composition and the mechanical properties of the welded material, the surface roughness and the metal sheet geometry) need to be suitable for establishing a joint by ultrasonic welding [3, 4].

3. Recrystallization

Ultrasonic welding is a useful joining tech-nology for the welding of thin sheets. During this process high temperatures are created which cause recrystallization.

The recrystallization depends on the follow-ing:
– heating temperature (a thermal activated process);
– heating rate;
– heating time;
– plastic deformation;
– deformation rate;
– original grain size;

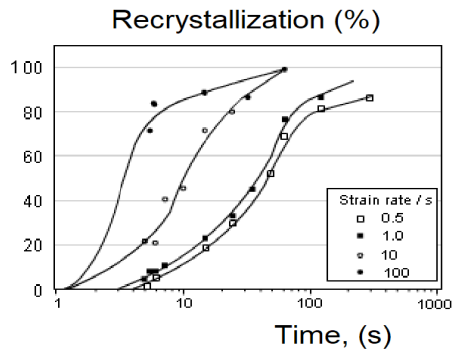

Figure 1. *Relationship between recrystallization and the strain rate [5]*

– secondary phases;
– solute alloy contents;
– texture before deformation.

The welding process causes a high rate of de-formation because it uses high frequency ul-trasound. The applied frequency (20 000 Hz) causes a high rate of friction and a high rate of plastic deformation. The higher plastic defor-mation rate generates faster recrystallization (**Figure 1**).

It is known that recrystallization principally depends on the heating temperature and the heating time. No high temperature or long retention time was observed in our experi-ments, however, the structure was altered (particle size and grain geometry changed) [6, 7].

4. Experiments

The experiments were carried out with dif-ferent welding times; the welded pieces are showed on the **Figure 2.**

The welding times are summarised in **Table 1.** The material used was aluminum (EN 485-2:2016).

The other welding parameters used are shown in the **Table 2** The visual test results of (Number 1-3) pieces were acceptable. In the case of the (Number 4-6) pieces, the defor-mation grades were more than acceptable.

The surface of sample 6 is burnt, which sug-gests overheating. The pieces which were ob-servable by visual test, were tested by tensile test and the joint cross section tested by mi-croscopy.

The microscopy test showed that the micro-structure had changed. **Figure 3** shows the changes to the microstructure. The longer welding time and higher temperature caused recrystallization, grain deformation and grain coarsening in the joint and in the heat affected zone.

Figure 2. *Different welding time effects in the case of ultrasonic welded joints*

Table 1. *Welding times (ms)*

Sample number	Welding time [ms]
1	110
2	220
3	330
4	440
5	660
6	880

Table 2. *Welding parameters*

Trigger Force	400 N
Pressure management	400 ms
Amplitude	86%
Initial pressure	0.3 bar
Welding pressure	5 bar

5. Results and conclusions

High frequency ultrasonic welding causes heat and plastic deformation. The heat and the defor-mation produce changes in the micro-structure of the tested materials. The defor-mation rate is unknown because of the high frequency friction.

Recrystallization can't be explained by traditional concepts in the case of this process, because the welding time applied is very short; only 110-880 ms.

Further analysis of the resulting microstruc-ture is necessary in order to understand the causes. It could be supposed that the resulting microstructure was created not only by the heat but also by the high rate of plastic deformation. It has been found that in the case of ultrasonic welding, cold and / or hot forming was done depending on the welding temperature.

Acknowledgement

The authors acknowledge the financial support of the Hungarian State and the European Union under the EFOP-3.6.1-16-2016-00010 project.
Furthermore, we want to tell thanks to Mihaly Szilágyi for his technical support in case of testing.

References

[1] Bagyinszki Gy., Bitay E.: *Hegesztéstechnika II. Berendezések és mérések.* EME, Kolozsvár/Cluj, 2010.
http://hdl.handle.net/10598/15438

[2] Bagyinszki Gy., Bitay E.: *Hegesztéstechnika I. Eljárások és gépesítés.* EME, Kolozsvár/Cluj, 2010.
http://hdl.handle.net/10598/15437

[3] Kovács T.: *Investigation of the ultrasound welded aluminium joint microstructure*. Lecture Notes in Mechanical Engineering 49. (2018) 735–741.
https://doi.org/10.1007/978-3-319-75677-6_62

[4] Szilágyi M., Kovács T.: *Ultrahang hegesztés alkalmazása alumínium lemeznél.* In: Proceedings of 8th International Engineering Symposium at Bánki. Budapest, Magyarország, 2016.
http://bgk.uni-obuda.hu/iesb/2016/publication/55.pdf

[5] Callister Jr. W. D., Rethwisch D. G.: *Materials science and engineering. An introduction.* 8th ed., John Wiley & Sons Inc., USA, 2000.

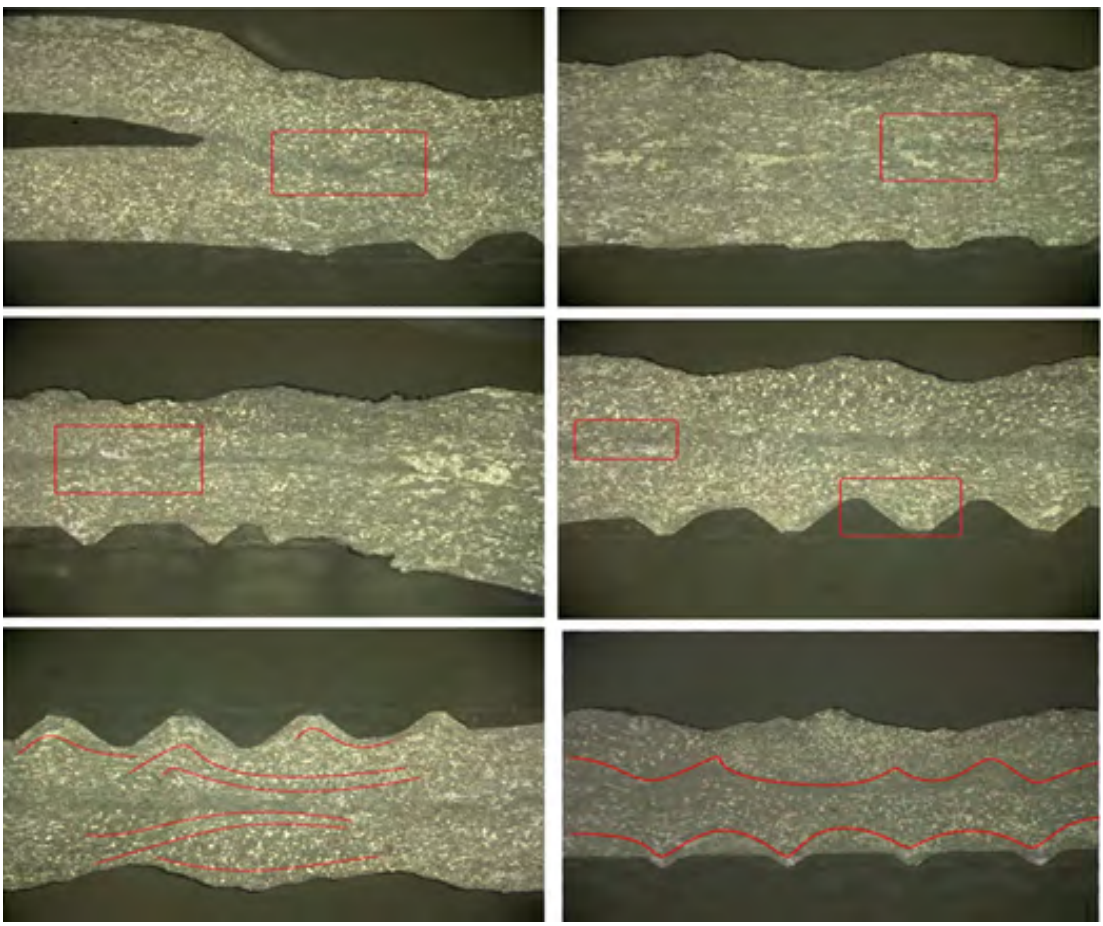

Figure 3. *Ultrasonic welded joint microstructure*

[6] Astashev V. K., Babitsky V. I.: *Ultrasonic processes and machines, dynamics, control and applications*. Springer-Verlag, Berlin–Heidelberg, 2007.
[7] Chen K., Zhang Y.: *Mechanical analysis of ultrasonic welding considering knurl pattern of sonotrode tip*. Materials&Design, 87. (2015) 393–404. https://doi.org/10.1016/j.matdes.2015.08.042

Acta Materialia Transylvanica 1/1. (2018) 53–56.
https://doi.org/10.2478/amt-2018-0018
Hungarian: ~~https://doi.org/10.2478/amt-2018-0017~~
https://doi.org/10.33923/amt-2018-0017
Corrected: 29.08.2023.

Surface Roughness Effect in the Case of Welded Stainless Steel Corrosion Resistance

László TÓTH[1], Ferenc HARASZTI[2], Tünde KOVÁCS[3]

[1, 3] *Óbuda University, Bánki Donát Faculty of Mechanical and Safety Engineering, Department of Materials Technology, Budapest, Hungary, toth.laszlo@bgk.uni-obuda.hu, kovacs.tunde@bgk.uni-obuda.hu*

[2] *Óbuda University, Bánki Donát Faculty of Mechanical and Safety Engineering, Doctoral School of Safety and Security Science, haraszti.ferenc@bgk.uni-obuda.hu*

Abstract

It is known that fusion welding can cause a decrease in the corrosion resistance of the heat affected zone of unstabilized stainless steels. The reason for this problem is that the welding heat (in the heat affected zone (HAZ)) can cause chromium-carbide (Cr23C6) precipitation with the simultaneous reduction of chromium content at the local grain boundaries. The chromium content dictates the corrosion resistance level. The relationship between surface roughness and corrosion behaviour is well known. We sought to find the difference between the corrosion resistance and surface roughness relationship in the case of cold rolled stainless steel and in the case of heat treated (welding heat effect simulated) stainless steel [1-3].

Keywords*: corrosion, precipitation, corrosion resistance, surface roughness, heat affected zone (HAZ).*

1. Introduction

Stainless steels are very useful and popular in the industrial and civil engineering fields. There is a wide variety of stainless steels each having different properties and chemical composition. The austenitic stainless steels, due to their chemical composition, have high ductility and high corrosion resistance. Heat can cause some precipitation in the micro-structure, and this decreases the corrosion resistance level [4, 5].

The effects of surface roughness on the behaviour of steel in the presence of corrosion is well understood: Corrosion is more aggres-sive in the case of the high surface roughness steels than in case of those with low roughness [6, 7]. Due to chemical composition, the cold rolling of steel sheets creates a thin corrosion-resistant passive layer. For aesthetic purposes, the building industry often requires grinding of the steel surface. This gives a nice finish to the sheet's surface. However, it also decreases the corrosion resistance as the protective layer is removed and the surface roughness changes.

Theoretically, the resistance layer renews rapidly on the surface of stainless steels, but this process is inhibited by the grinding pro-cess, causing the corrosion resistance to de-crease [8].

2. The experimented steel

2.1. Austenitic stainless steel (1.4307)

The chemical composition of the used aus-tenitic steel is shown in **Tabel 1.** High carbon affinity elements (eg. Ti, Ta, Nb) are not found in this chemical composition and the carbon contain is low.

The level of corrosion resistance of this steel is very high. The pitting resistance equivalent numbers (PREN) are calculated by the following most common equation, with the element weight as a percentage.

$$PREN=Cr+3.3\ Mo+16\ N \quad (1)$$

$$PREN=19.74 \quad (2)$$

2.2. Surface preparation

The tested sample surfaces were cleaned and ground according to grain size and the same chemical composition (Al_2O_3) of the grinding

Table 1. *The used steel chemical composition in weight percentage (the rest is iron) (%)*

C	Mn	S	P
0.026	1.71	0.004	0.004
Si	**Ni**	**Cr**	**N**
0.23	8.15	18.3	0.09

papers. The used paper parameters are shown in the **Table 2**. The grinding process created different surface roughness in the case of the tested samples. The surface roughness (Ra) of the samples was different, results shown in **Table 2**.

2.3. Heat treating

In the case of stainless steels, the fusion welding process is a very common joining technology. Fusion welding technology pro-duces a high heat effect during the joining process, which can change the microstructure in the heat affected zone (HAZ). We heated all samples for one hour at 800 ºC and cooling was by air. .

Table 2. *The used grinding paper parameters and the surface roughness of the ground sheets*

	1	2	5	6
Grinding Paper	P120	P180	P320	P400
Surface roughnes Ra (µm)	2.353	1.412	0.677	0.54

3. Corrosion tests

The surface roughness and heat caused changes in both microstructure and corrosion resistance. This process was modelled by la-boratory experiments [9–11]. The tested samples were treated in FeIIICl solution (ASTM A 262), for 96 hours at 30 ºC. Under this load, the sheets showed a weight loss that is measurable with analytical scales [12]. The measured weight loss volumes (g) are shown in the **Table 3.**

Tested samples were examined by microscopy and the results are shown in **Figure 1-4.** On the surface we detected pitting corrosion phenomena through visual testing, we used stereo microscopy, (100x magnification **Figure 1-4**) the figures show a 10x10mm area of the test samples.

We detected that in the case of the tested samples the unsuitable surface roughness caused reduced corrosion resistance. In the case of the heat treated samples, the heat treatment decreased corrosion resistance. (**Figures 1–4**) show the heat treated different surface roughness samples after corrosion tests. The corrosion was recognizable by visual testing and measurable by weight loss control.

4. Conclusions

We have concluded on basis of our experi-mental results that the corrosion resistance of the ground surface samples was lower than that of the cold rolled samples.

We also concluded that the corrosion weight loss in case of the heat treated samples was higher than in case of the others.

I. We found a relationship between surface roughness and weight loss in the tested samples.
II. Heat treating caused the decreasing of cor-rosion resistance.

Table 3. *Weight loss of the tested samples*

Number	Without heat treating	Heat treated
1	0.4217 g	0.9608 g
2	0.4005 g	1.2904 g
5	0.4468 g	1.0636 g
6	0.561 g	1.7667 g

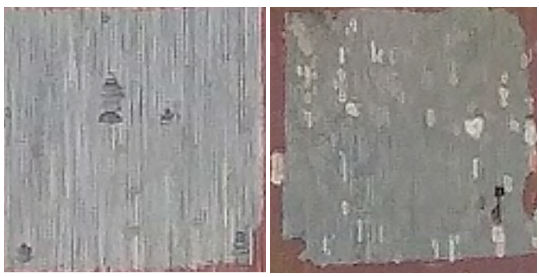

Figure 1. *N. 1. samples: a) without heat treating, b) heat treated*

Figure 2. *N. 2. samples: a) without heat treating, b) heat treated*

Figure 3. *N. 5. samples: a) without heat treating, b) heat treated*

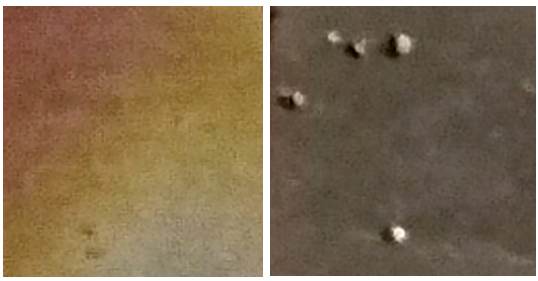

Figure 4. *N. 6. samples: a) without heat treating, b) heat treated*

III. We detected that in the case of the stain-less steel samples, surface grinding negatively affects corrosion resistance. Between surface roughness and corrosion resistance, we found a measurable correlation in the case of the tested samples.

IV. We carried out our test immediately after surface grinding and consequently, the protective surface layer was not able to re-cover in this short time. We assume that after surface grinding the protective layer can renew but requires a longer time.

These results are very important and there-fore further research is needed in order to better understand the surface properties of stainless steels.

Acknowledgement

The authors acknowledge the financial support provided by the Hungarian State and the European Union under the EFOP-3.6.1-16-2016-00010 project.

References

[1] Haraszti F., Kovács T.: *Plastic deformation effect of the corrosion resistance in case of austenitic stainless steel.* IOP Conference Series: Materials Science and Engineering, 175. (2017). https://doi.org/10.1088/1757-899X/175/1/012048

[2] Tedmon Jr. C. S., Vermilyea D. A., Rosolowski J. H: *Intergranular corrosion of austenitic stainless steel.* Journal of the Electrochemical Society, 118/2. (1971) 192–202. https://doi.org/10.1149/1.2407966

[3] Bagyinszki Gy., Bitay, E.: *Hegesztéstechnika II. Berendezések és mérések.* EME, Kolozsvár/Cluj, 2010. http://hdl.handle.net/10598/15438

[4] Haraszti F., Kovács T.: *Galvanic corrosion occurs heat experiments by thermographic camera.* IOP

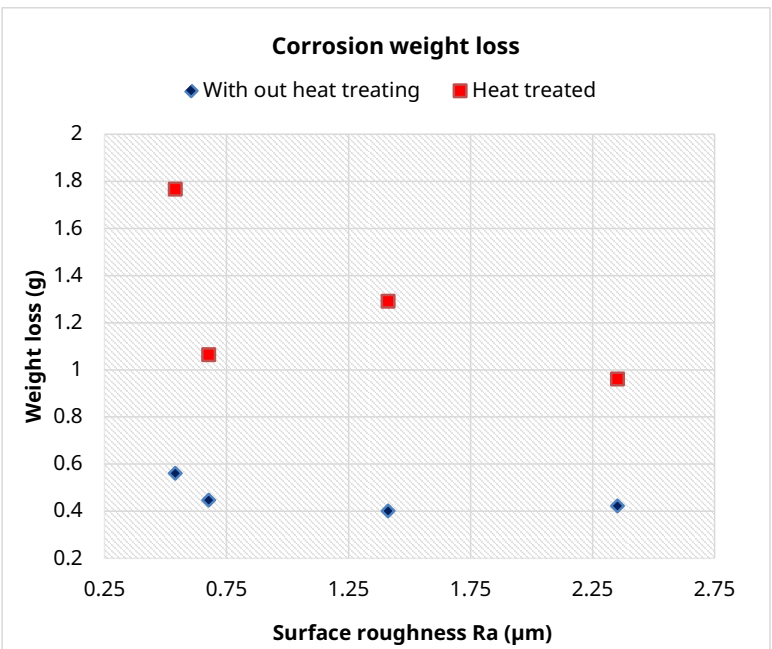

Figure 5. *Corrosion effected weight loss in the case of heat treated and non-heat treated samples*

Conference Series: Journal of Physics: Conf. Series 1045. (2018). https://doi.org/10.1088/1742-6596/1045/1/012016

[5] Haraszti F: *Korrózió vizsgálatok alapjai.* In: A XXI. Fiatal műszakiak tudományos ülésszak előadásai. Proceedings of the 21th international scientific conference of youngth engineers. Műszaki Tudományos Közlemények 5., EME, Kolozsvár/Cluj, România, 2016. 189–192. http://hdl.handle.net/10598/29058

[6] Kovács T., Kuzsella L.: *High energy rate forming induced phase transition in austenitic steel.* Journal of Physics Conference-Series, 790. (2017). https://doi.org/10.1088/1742-6596/790/1/012039

[7] Szigeti Á., Kovács-Coskun T.: *Magas hőmérsékletű korrozív közegben üzemelő acélrugó gyártástechnológiai tervezése.* In: A XXI. Fiatal műszakiak tudományos ülésszak előadásai. Proceedings of the 21th international scientific conference of youngth engineers. Műszaki Tudományos Közlemények 5., EME, Kolozsvár/Cluj, România, 2016. 377–380. http://hdl.handle.net/10598/29111

[8] Dománkova M., Kocsisová E., Slatkovský I., Pinke P.: *The microstructure evolution and its effect on corrosion properties of 18Cr-12Ni-2,5Mo steel annealed at 500–900 °C.* Acta Polytechnica Hungarica, 11/3. (2014) 125–137. https://www.uni-obuda.hu/journal/Domankova_Kocsisova_Slatkovsky_Pinke_49.pdf

[9] Nyikes Z., Rajnai Z.: *Big Data, as part of the critical infrastructure.* 2015 IEEE 13th International Symposium on Intelligent Systems and Informatics (SISY), Subotica, Serbia, 2015. 217–222. https://doi.org/10.1109/SISY.2015.7325383

[10] Reti T., Kovacs T.: *A phenomenological method for the prediction of damage accumulation processes under varying external conditions.* In: Materials Science Forum, 414–415. (2003) 317–322. https://doi.org/10.4028/www.scientific.net/MSF.414-415.317

[11] Tokody D., Flammini F.: *Smart systems for the protection of individuals*. Key Engineering Materials, 755. (2017) 190–197. https://doi.org/10.4028/www.scientific.net/KEM.755.190

[12] ASTM Standard Practice in A 262 for Detecting Susceptibility to Intergranular Corrosion in Austenitic Stainless Steels (1995).

Acta Materialia Transylvanica 1/1. (2018) 57–60.
https://doi.org/10.2478/amt-2018-0020
Hungarian: ~~https://doi.org/10.2478/amt-2018-0019~~
https://doi.org/10.33923/amt-2018-0019
Corrected: 29.08.2023.

Metal Foam Analysis Based on CT Layers

Tamás Antal VARGA,[1] Tamás MANKOVITS[2]

University of Debrecen, Faculty of Engineering, Department of Mechanical Engineering, Debrecen, Hungary

[1] *varga.tamas@eng.unideb.hu*

[2] *tamas.mankovits@eng.unideb.hu*

Abstract

The geometrical modelling of metal foams remains one of the greatest challenges facing researchers in the field. In this paper the analysis of the inner structure of closed-cell aluminium foam - an essential part of the construction of an idealized foam model - is presented. With the application of special purpose software the properties of the foam cells can be mapped precisely and the results applied to the development of idealized foam geometry constructed in CAD applications.

Keywords*: metal foam, CT, analysis, structure.*

1. Introduction

Metal foams are relatively new and advanced materials with high stiffness to weight ratio, good thermal conductivity, good acoustic insulation and excellent energy absorption capability. This makes them ideal materials for a wide variety of applications [1–4]. Therefore, they have been increasingly employed in applications such as structural elements, automotive parts, sound and vibration absorbers and even biomedical implants [5–8], Basically, the mechanical properties of metal foams are influenced by three dominant factors [9–13]. the properties of the solid phase, the relative density of the solid phase and the spatial arrangement of the cells, that is, the structure of the metal foam (cell distribution, cell shape). The understanding of the structure – property correlations in metal foams is required for optimizing its mechanical performance for a given application [9–14].

2. Analysis of metal foam structure based on computer tomography

With the help of computer tomography several analytic tests can be carried out with suitably dedicated software, allowing the attributes of the cells constituting the metal foam to be mapped. The metal foam investigated is a closed cell aluminium foam, which can be seen in **Figure 1**. The size of the 3D sample model is 14×14×14mm^3.

The shots made by the CT are imported into the dedicated software. The accuracy of the tests only relies on the accuracy of the CT device. The following attributes provide useful information regarding the metal foam's inner structure: the position of the cells (the X, Y and Z coordinates of the centre of gravity), the size of the cells (the cell's volume and surface), and the form of the cells (how spheroidal the cell is). The software can determine these data thereby allowing us to identify the internal structure of the metal foam; moreover, these are the input data of the idealized 3D models.

The software is capable of visual display; hence more detail can be analysed including the segments of cells. After the performed analysis, we acquired the quantified data of cells and could also observe them visually as shown in **Figure 2**. During the analysis, the software detected 686 cells based on the parameters that we provided.

In **Figure 2** we can see that the software falsely detected some cells outside of the perimeters of the 3D sample. This happened due to the fact that the 3D sample's outer surface is not homogenous; hence the software detected the open cells on the surface to which it assigned volume. These falsely detected cells can be detected with filtering, since the volume of these cells is much greater than the

real cells constructing the metal foam. The basis of filtering could also be the centre of gravity of those cells outside the 3D sample, allowing them to be easily removed from the results of the analysis.

After filtering, the falsely detected cells became inactive leaving only the real cells in the model. 25 cells were removed thanks to the filter, hence in our main analysis 661 cells were examined. From the data acquired, it is possible to measure the dispersion of the cells' volume by size (**Figure 3**), and the dispersion of the spheroidicity (**Figure 4**) of the cells. It is shown by the dispersion of the cells' volume that nearly 60% have a volume of 0-2 mm^3, while there are specifically large volume cells as well. The spheroidicity of cells varies from 0-1, in which 1 represents the sphere attribute. From the analysis of the metal foam's inner structure it was shown that the cells are rather ellipsoid or general in shape, which raises further questions regarding the planning of the idealized model.

However, **Figure 4** clearly shows that the cells have nearly the same spheroid attribute.

3. Conclusions

Our research has shown that CT shots of the given geometry are a necessary element of the analysis and modelling of metal foams. With the structure-analysing software we have the possibility to detect the place, size and form of the cells constituting the metal foam. We also have the opportunity to model even more phased metal

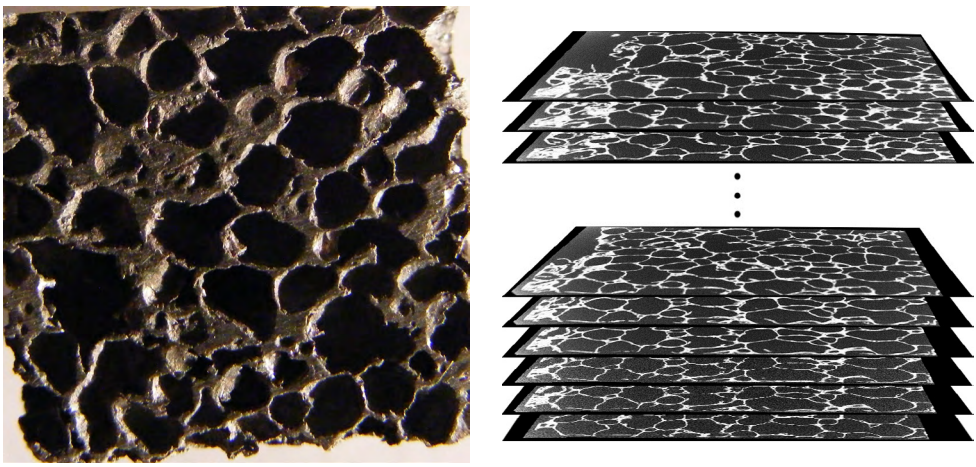

Figure 1. *Closed cell aluminium foam 3D sample model and the shots made by the CT*

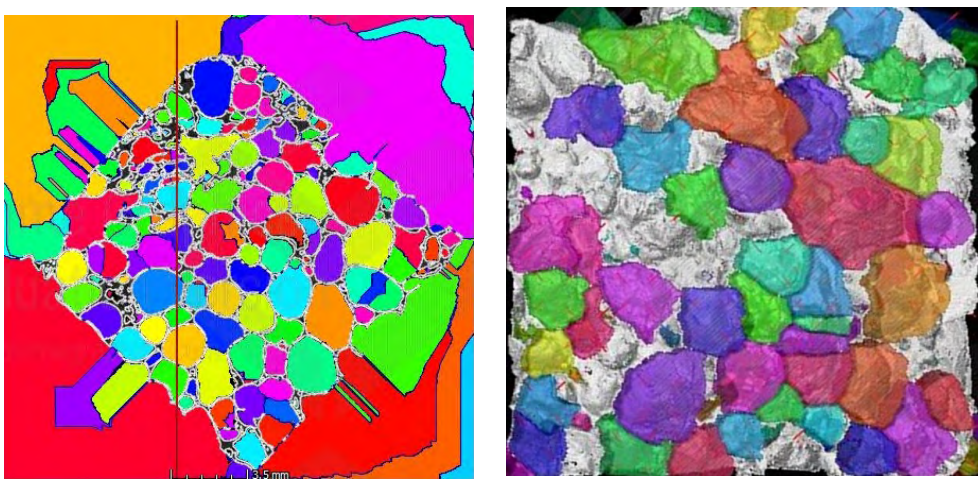

Figure 2. *Cells detected before and after filtering*

foams, in terms of real geometry. Most probably this is the best process available for analysing our metal foam, its only disadvantage being the need for a CT device and (due to the fact that these processes demand high computing capacity) a high performance modelling computer.

Acknowledgements

This research was supported by the ÚNKP-4 New National Excellence Program of the Ministry of Human Capacities of Hungary.

References

[1] Ashby M. F., Evans A. G., Fleck N. A., Gibson L. J., Hutchinson J. W., Wadley H. N. G.: *Metal foams. A design guide*. Butterworth-Heinemann, 2000.

[2] Mankovits T., Budai I., Balogh G., Gábora A., Kozma I., Varga T., Manó S., Kocsis I.: *Structural analysis and its statistical evaluation of a closed-cell metal foam.* International Review Applied Science Engineering, 5/2. (2014) 135–143. https://doi.org/10.1556/IRASE.5.2014.2.5

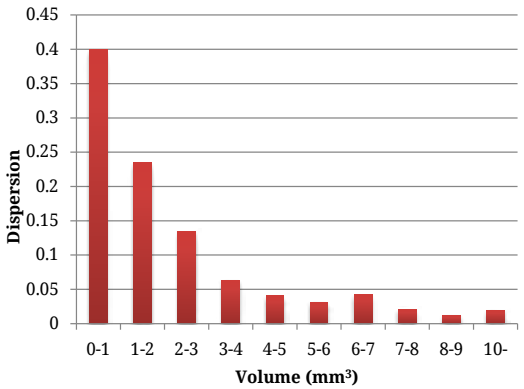

Figure 3. *The dispersion of cell volume*

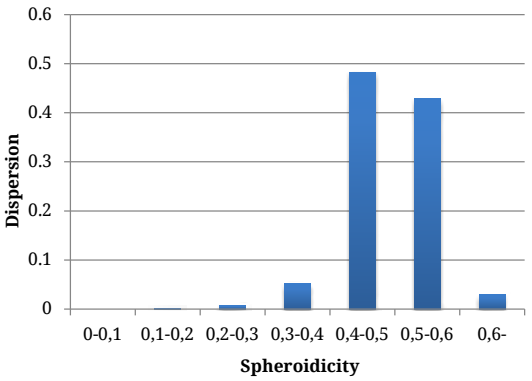

Figure 4. *The dispersion of the spheroidicity of cells*

[3] Orbulov I. N.: *Compressive properties of aluminium matrix syntactic foams*. Materials Science and Engineering A, 555. (2012) 52–56. https://doi.org/10.1016/j.msea.2012.06.032

[4] Orbulov I. N., Májlinger K.: *Description of the compressive response of metal matrix syntactic foams.* Materials and Design, 49. (2013) 1–9. https://doi.org/10.1016/j.matdes.2013.02.007

[5] Kou D. P., Li J. R., Yu J. L., Cheng H. F.: *Mechanical behavior of open-cell metallic foams with dual-size cellular structure.* Scripta Materialia, 59/5. (2001) 483–486. https://doi.org/10.1016/j.scriptamat.2008.04.022

[6] Jang W. Y., Kyriakides S., Kraynik A. M.: *On the compressive strength of open-cell metal foams with Kelvin and random cell structures.* International Journal of Solids and Structures, 47/21. (2010) 2872–2883. https://doi.org/10.1016/j.ijsolstr.2010.06.014

[7] Lu Z.-X., Liu Q., Huang J.-X.: *Analysis of defects on the compressive behaviors of open-cell metal foams through models using the FEM*. Materials Science and Engineering A, 530. (2011) 285–296. https://doi.org/10.1016/j.msea.2011.09.088

[8] An Y., Wen C., Hodgson P. D., Yang C.: *Investigation of cell shape effect on the mechanical behaviour of open-cell metal foams.* Computational Materials Science, 55. (2012) 1–9. https://doi.org/10.1016/j.commatsci.2011.11.030

[9] Maire E., Fazekas A., Salvo L., Dendievel R., Youssef S., Cloetens P., Letang J. M.: *X-ray tomography applied to the characterization of cellular materials. Related finite element modeling problems.* Composites Science and Technology, 63. (2003) 2431–2443. https://doi.org/10.1016/S0266-3538(03)00276-8

[10] Jirousek O., Doktor T., Kytyr D., Zlámal P., Fíla T., Koudelka P., Jandejsek I., Vavrík D.: *X-ray and finite element analysis of deformation response of closed-cell metal foam subjected to compressive loading.* Journal of Instrumentation, 8/2. (2013). https://doi.org/10.1088/1748-0221/8/02/C02012

[11] Youssef S., Maire E., Gaertner R.: *Finite element modelling of the actual structure of cellular materials determined by X-ray tomography.* Acta Materialia, 53/3. (2005) 719–730. https://doi.org/10.1016/j.actamat.2004.10.024

[12] Veyhl C., Belova I. V., Murch G. E., Fiedler T.: *Finite element analysis of the mechanical properties of cellular aluminium based on microcomputed tomography*. Materials Science and Engineering A, 528. (2011) 4550–4555. https://doi.org/10.1016/j.msea.2011.02.031

[13] Jeon I., Asahina T., Kang K.-J., Im S., Lu T. J.: *Finite element simulation of the plastic collapse of closed-cell aluminum foams with X-ray computed tomography*. Mechanics of Materials, 42. (2010) 227–236. https://doi.org/10.1016/j.mechmat.2010.01.003

[14] Mankovits T., Varga T. A., Manó S., Kocsis I.: *Compressive response determination of closed-cell aluminium foam and linear-elastic finite element simulation of μCT-based directly reconstructed geometrical models.* Strojniški vestnik. Journal of Mechanical Engineering, 64/2. (2018) 105–113. https://doi.org/10.5545/sv-jme.2017.5048

ACTA MATERIALIA TRANSYLVANICA 2018

ERRATUM

Az Erdélyi Múzeum-Egyesület mint kiadó és az Acta Materialia Transylvanica szerkesztősége sajnálattal értesíti a szerzőket és az olvasókat, hogy a folyóirat 2018-as évfolyam 1 és 2. lapszámaiban a cikkek magyar nyelvű változatainál a DOI-azonosítók prefixei hibásan jelentek meg.

A cikkek fejléceiben a magyar nyelvű változatnak megfelelő DOI prefix helyesen: **10.33923**, nem 10.2478.

A prefixek 2023 szeptemberében a lapszámok honlapján:

https://eme.ro/publication-hu/acta-mat/acta2018-1.htm illetve

https://eme.ro/publication/acta-mat/acta2018-1.htm

és

https://eme.ro/publication-hu/acta-mat/acta2018-2.htm illetve

https://eme.ro/publication/acta-mat/acta2018-2.htm

minden cikkben javításra kerültek, feltüntetve az eredeti, hibás és az új, helyes azonosítót is.

A DOI-azonosítók helyes számra történő cserélése a Magyar Tudományos Művek Tárában (MTMT) is megtörtént.

A hibáért minden szerző és olvasó szíves elnézését kérjük és tisztelettel kérjük, hogy ezentúl az új, helyes azonosítót legyenek szívesek használni!

Az Erdélyi Múzeum-Egyesület Kiadó és az Acta Materialia Transylvanica Szerkesztősége nevében:

Bitay Enikő

főszerkesztő

Kolozsvár, 2023. 09. 01.

ACTA MATERIALIA TRANSYLVANICA 2018

ERRATUM

The Erdélyi Múzeum-Egyesület as Publisher, and the Editorial Office of Acta Materialia Transylvanica regret to inform the authors and readers that the prefixes of the DOI identifiers of the Hungarian versions of the articles in issues 1 and 2 of the journal in 2018 were incorrectly published.

In the article headings, the DOI prefix corresponding to the Hungarian version of the article is **10.33923**, not 10.2478.

In September 2023, the prefixes were corrected in all articles on the websites of the journal issues:

https://eme.ro/publication-hu/acta-mat/acta2018-1.htm respectively

https://eme.ro/publication/acta-mat/acta2018-1.htm

and

https://eme.ro/publication-hu/acta-mat/acta2018-2.htm respectively

https://eme.ro/publication/acta-mat/acta2018-2.htm

showing the original incorrect one crossed out and the new, correct identifier.

The replacement of the DOI identifiers with the correct number has also been done in the Hungarian Repository of Scientific Works (MTMT).

We apologize to all authors and readers for this error, and respectfully request that you use the new, correct identifier from now on!

On behalf of the Erdélyi Múzeum-Egyesület Publisher and the Editorial Office of Acta Materialia Transylvanica:

Bitay Enikő

Editor-in Chief

Cluj-Napoca, 1st September, 2023.